Elasticity of the Lens Capsule as Measured by Osmotic Swelling

A THESIS
SUBMITTED TO THE FACULTY OF THE GRADUATE SCHOOL
OF THE UNIVERSITY OF MINNESOTA
BY

Tracy A Powell

IN PARTIAL FULFILLMENT OF THE REQUIREMENTS
FOR THE DEGREE OF
MASTER OF SCIENCE

Victor H Barocas

June 2010

Acknowledgements

I extend my deepest gratitude to my advisor, Victor Barocas. He has provided guidance and assistance throughout my graduate education and research and unparalleled interest and concern for my future. I also thank my thesis committee members, Yoav Segal and Kevin Dorman, for their weekly guidance of the project, Rouzbeh Amini for his foundational work on the project, and Alina Oltean and Vincent Barnett for their contributions to the porcine work. The encouragement and advice from the Barocas Laboratory group also played an integral role in the success of my thesis research.

The technical assistance of Edward A. Sander is also gratefully acknowledged, as is generous provision of *post-mortem* porcine eyes by Visible Heart® Laboratory and Experimental Surgical Services at the University of Minnesota and of mouse eyes used for methodology development by Chun Wang's Laboratory. This work was supported by the National Institutes of Health (R01-EY015795, R21-GM082823) and with resources and the use of facilities at the Minneapolis VA Medical Center.

Abstract

As an alternative to purely mechanical methods, optical tracking of passive osmotic swelling was used to assess mechanical properties of the ocular lens capsule. Although limited by being a single measurement on a heterogeneous tissue, osmotic swelling provides a quantitative assessment of the stiffness of the lens capsule without requiring dissection or manipulation of the lens. A simple model was developed accounting for the permeability of the lens fiber cells and capsule to water, the concentration of fixed charges in the fiber cells, and the capsule's resistance to the swelling of fiber cells. Fitting the model solution to experimental data provided an estimate of the elastic modulus of the lens capsule under the assumption of linear isotropic elasticity. The model was developed with the porcine lens to provide validity and was extended to a mouse model with X-linked Alport Syndrome, the most common form of the human disease that results in the absence of a collagen IV monomer normally present in the lens capsule. The calculated elastic moduli for the porcine lens is comparable to previously reported moduli of elasticity for the porcine lens capsule at small strains (<10%), and a slight increase with hypotonicity is consistent with the nonlinear mechanical behavior of the lens capsule. The calculated elastic moduli for the mouse lenses were similar between wild type and Alport and are comparable to a reported modulus of elasticity for rat lens capsules at small strains. The mouse lens modulus of elasticity showed a similar response to bath concentrations as the porcine lenses, increasing with hypotonicity. However, the difference in the tendency to rupture of the Alport and wild type lens capsules were statistically significant; for lenses that reached 14% strain in the equatorial direction, the Alport lenses had a greater tendency to rupture. This work will be extended to investigate the temporal effects of Alport syndrome on the elastic modulus and rupture mechanics of lens capsules. Osmotic challenge overcomes the size limitations of previously employed techniques for measuring the elastic modulus of the lens capsule and can provide insight into the properties of basement membranes through its application to other mutant mice.

Table of Contents

List of Tables

List of Figures

1. INTRODUCTION

1.1 Purpose

The long-term goal of this work is to use mechanical behavior to provide insight into the organization of different basement membranes by exploring how they are affected by the loss of one or more constituent proteins. The purpose of this thesis is to evaluate a testing method with the porcine model that utilizes osmotic pressure as a driving force to measure the elastic modulus of the ocular lens capsule and to investigate the change in elasticity of the lens capsule in mice with Alport syndrome as compared to wild type (WT) mice.

1.2 Background

Basement membranes are planar extracellular matrices that are ubiquitous within tissues and serve roles in the organization, support, and regulation of cell populations. The capsule surrounding the lens of the eye is an experimentally accessible basement membrane, accounting for its wide use as a model in studies of basement membrane biochemistry, structure, permeability, and mechanics [1-5]. The lens capsule is itself a mechanical structure regulating lens shape and a permeability barrier serving integrated mechanisms of ion and water transport [6-9]. Changes in the lens capsule have been implicated in pathological conditions including cataracts and morphologic abnormalities in genetic disorders of basement membranes [10-14].

The mechanical properties of basement membranes arise from their detailed molecular structures. While highly diverse, basement membranes are formed from a palette of

constituents that includes interwoven networks of type IV collagen and laminin, in which are embedded additional specialized components [15-18]. Growing knowledge of genetic disorders of basement membranes, coupled with genetic mouse models, affords new opportunities to relate the mechanical properties of basement membranes including the lens capsule to their molecular constituents. Knockout mice have been developed for perlecan [19], SPARC [20], and a minor collagen IV monomer [21].

Alport syndrome involves a mutation in a gene encoding one of the six collagen IV monomers present in basement membranes. The monomers form heterotrimers; the heterotrimer affected in Alport syndrome is primarily localized to the kidney, ear, and lens capsule [21]. Mice with Alport syndrome die prematurely due to failure of the kidney basement membrane, but they live past the eight-week duration for development given in this experiment. Type IV collagen is only found in basement membranes [22], so the mechanical effects of Alport Syndrome are specific to basement membranes. When comparing different basement membranes, the only structural collagen protein universally present is collagen IV [22].

1.3 Related Work

Methods previously utilized for determining the mechanical properties of lens capsules in pigs, cows, and humans require dissection or manipulation of the lens capsule: ring pulling [23,24], pressure-volume/ volume-strain methods [25-27], and controlled inflation [7,28]. These techniques are not well suited for mice due to the small lens size. Osmotic swelling overcomes the manipulation difficulties of the mouse lens and allows

for multiaxial testing while keeping the lens and lens capsule in their native geometry. The elastic modulus for the porcine model has been determined through some of these mechanical techniques [23,27], giving our model a basis for validity. Atomic force microscopy (AFM) has also been used [29], but it is an expensive procedure and may not correctly determine the elastic modulus.

Osmotic swelling has been used to measure mechanical and transport properties of cellular and subcellular membranes in animals and plants. Determination of the elastic modulus of cellular and mitochondrial membranes of sea urchin eggs [30], the permeability coefficient of human red blood cells [31], and plant cell mechanics both in the presence [32] and in the absence [33] of the cell wall are just a few examples. Similar to our model for the lens capsule, plant models have been developed that use osmotic pressure as the expansive force and mechanical pressure of the cell wall as the resistive force to cellular swelling [34,35].

Osmotic swelling of the isolated lens is also well established [14,36-38], primarily as a tool to explore lens physiology. The potential has been established for osmotic swelling as a tool to explore lens capsule stiffness [14]; however, there has been no previous osmotic-based determination of the lens capsule modulus of elasticity.

2. METHODOLOGY

2.1 Experimental System

2.1.1 Porcine

Porcine eyes were dissected from euthanized animals 1 to 8 hours *post mortem* (Visible Heart® Laboratory and Experimental Surgical Services at the University of Minnesota). The lenses were removed from the eyes and cleaned while submerged in Dulbecco's Phosphate Buffered Saline (DPBS) solution, which is isotonic to the lens cytoplasm (about 0.9% w/v). The lenses were then transferred anterior side-down to a closed chamber containing 0.1%, 0.2%, or 0.5% (w/v) NaCl and no energy source. Lenses thus subjected to passive osmotic challenge were digitally imaged every 5 to 10 minutes for 10 hours by a 1.3 mega-pixel camera mounted on an eyepiece adapter of a *4X Olympus* dissection microscope. Fiber optic lighting created a contrast between the lens and the black mat that is necessary for data analysis. Lens diameter was determined as the maximum distance between two points on the perimeter using MATLAB routines (Fig. 1) and lens volume calculated assuming spherical geometry. See Appendix A I for MATLAB code: get_time_radius_TAP.

The pixel-to-metric conversion was achieved using a picture of a calibrated circle taken under the experimental microscope setting for each data set. This picture was not obtained in some early porcine experiments, so the initial lens radius for those cases (n=5) was taken to be 4600 μm, the average of those measured (n=26) after the methodology was corrected. A sensitivity study on the initial radius showed that r=4500 μm or 4700 μm yielded less than 3% difference in the fitted parameters.

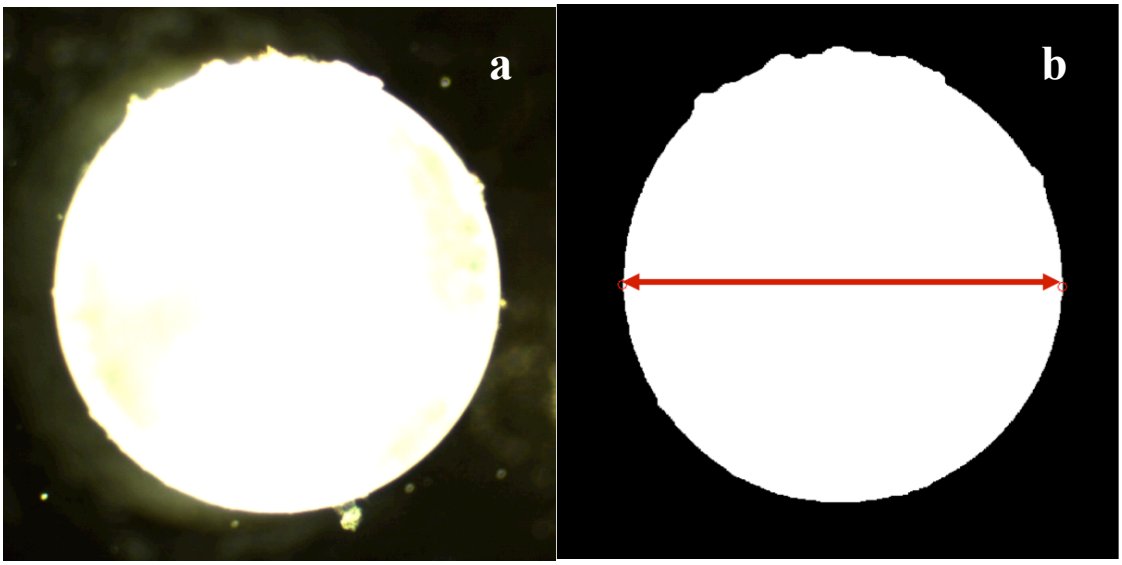

Figure 1: Porcine lens images. Image of a lens (a) captured from the camera during experiment and (b) after binomial conversion in MATLAB. Arrow indicates points from which the radius was calculated, depicted as small circles. The radius of this lens is 4.66 mm.

2.1.2 Mouse

Mouse lenses were dissected from euthanized males 15 to 30 minutes *post mortem* (male and initial female breeders provided by Jackson Laboratories; bred and housed in University of Minnesota RAR facilities) at 8 weeks of age +/- 3 days. The initial radii of the lens were obtained from a picture taken while the lens was in a covered dish with DPBS solution. The settings of the microscope were not changed after the initial picture; calibration was established from a picture of a calibrated circle. The lens was then placed in 0.1% or 0.3% NaCl solution, and a picture was taken every minute for three hours. The lenses were placed so that their sagittal plane was imaged, allowing for the measurement of the equatorial and sagittal diameter with the MATLAB routines (Fig. 2). See Appendix A I for MATLAB code: get_time_radius_TAP.

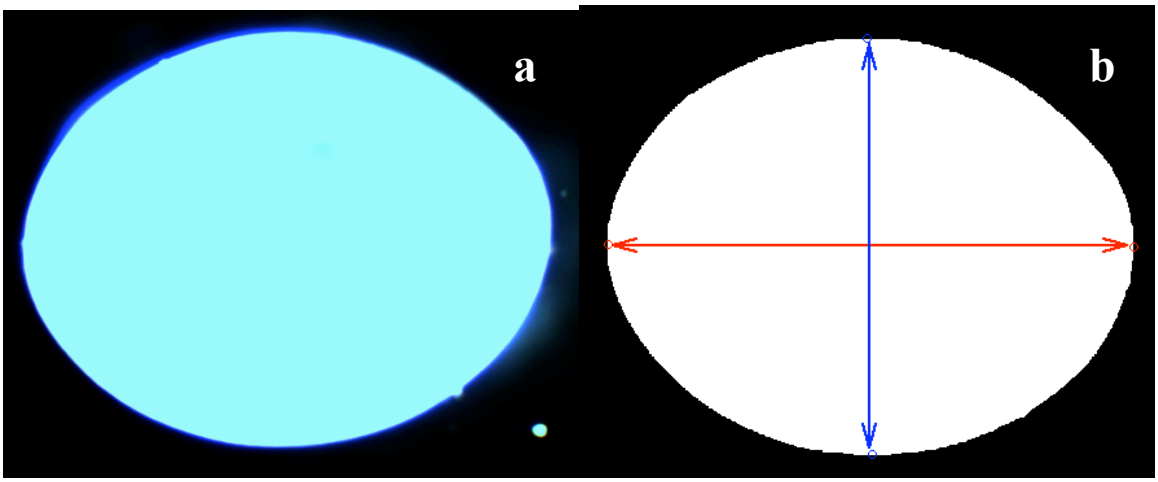

Figure 2: Mouse lens images. Image of a lens (a) captured from the camera during experiment and (b) after binomial conversion in MATLAB. The red and blue arrows indicate the points from which the equatorial radius and sagittal radius was calculated, respectively. The equatorial radius is 1.2 mm, and the sagittal radius is .94 mm.

Tail snips were taken *post mortem* at the time of the experiment. The tails were stored in an -80 degree freezer and sequenced after the data was analyzed, allowing for blind collection and analysis.

2.2 Analytical System

2.2.1 Physiological Model

The lens capsule surrounds the cellular lens, which has three regions (Fig. 3A): a central nucleus of mature fibers, surrounded by a cortex of differentiating fibers, which are separated from the lens capsule by epithelial cells along the anterior surface [39]. Water accumulation has been shown to occur in the epithelial and underlying lens fiber regions when placed in hypotonic solutions [36,40]. A waterfront is created as the lens

swells radially inward in layers; each layer appears to reach a fully swollen state before the next layer of fibers begins to swell [40]. This is expected, as the permeability to water molecules should increase significantly as the water content within the tissue increases. The waterfront in the lens capsule is similar to the immobilizing reaction modeled by Crank [41], and computational models have been constructed to determine the advancement of other naturally occurring fronts [42,43].

In our model, we consider passive transport only, neglecting the lens epithelial cells and dividing the lens fibers into two distinct regions. The *mushy zone* arises by osmotic swelling from the outer portion of the lens and is comprised of the swollen fibers (Fig. 3B & C). The *core* represents the remaining inner portion of the cellular lens that has not been reached by the waterfront.

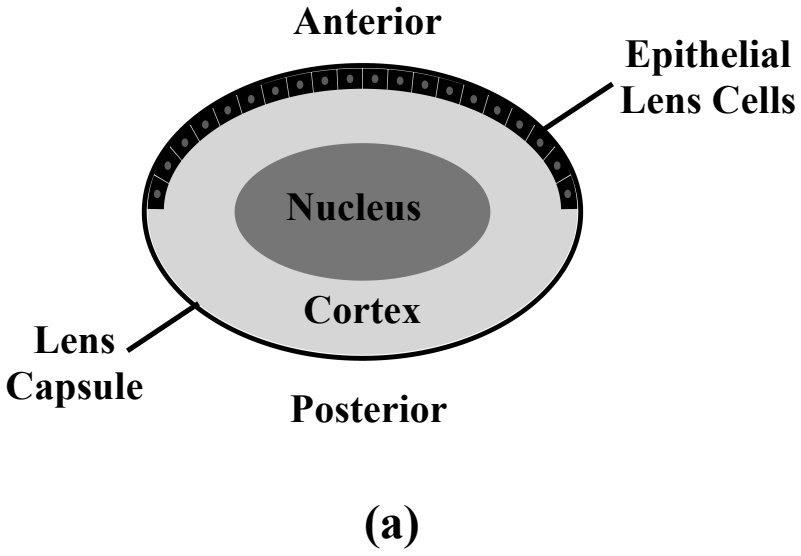

Figure 3: Anatomical and model schematic of ocular lens (continued on following page). (a) Anatomy of ocular lens.

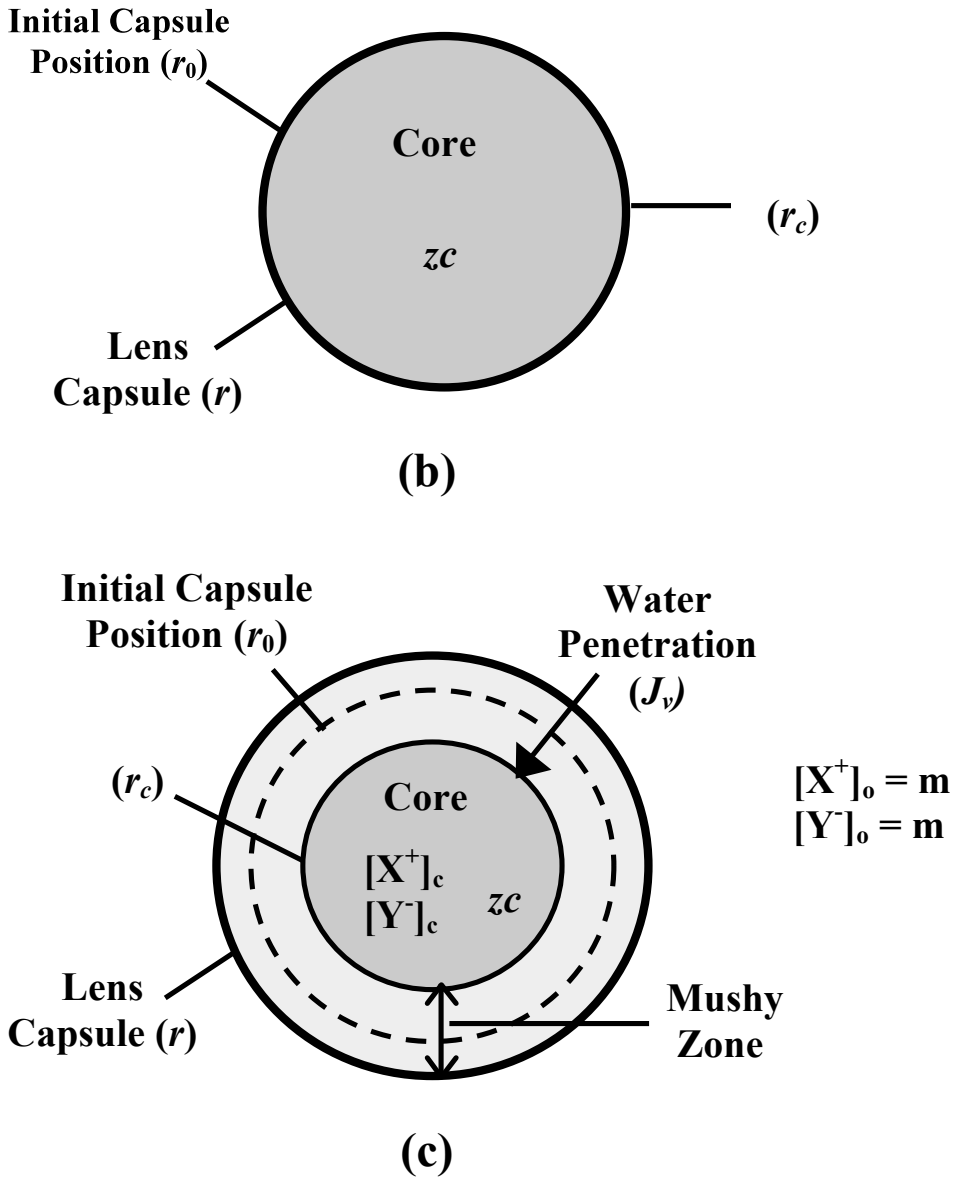

Figure 3: Anatomical and model schematic of ocular lens (continued from previous page). (a) Anatomy of ocular lens. (b) Model schematic of ocular lens before placement in hypotonic solution and (c) after some time in hypotonic solution. The subscripts *c* and *o* refer to the core of the lens and the outside bath, respectively. Initially the lens is not swollen and a mushy zone does not exist. After placement in hypotonic solution, water penetrates the lens capsule and the lens fibers swell in layers. The swollen fibers constitute the mushy zone, and the interface between the mushy zone and the core marks the waterfront. The difference in osmolarity between the core and outside bath is the driving force for lens expansion, which is opposed by mechanical pressure from the stretched lens capsule.

2.2.2 Model Transport and Mechanical Features

- The lens capsule is modeled as a thin, spherical shell of uniform thickness with linear elastic properties described by the mechanical theory of membranes [44] and water flux described by the Kedem-Katchalsky equation [45].
- The cellular lens is modeled as two regions: the mushy zone and the core. Water transport through the mushy zone is described empirically by Darcy's law.
- Without an energy source, transport through the lens is passive. Although multicellular, the mushy zone and core are each lumped and regarded as homogeneous.
- Two forms of charged species are present in the system. Biomacromolecules within the lens fiber cells that cannot cross the fiber cell membranes (including, for example, crystallins) have a constant fixed charge density *zc* within the core [46] and exert a Donnan effect [47]. Small ions (e.g. Na^+, Cl^-) are represented as monovalent and freely permeant [48].
- The osmotic pressure difference between the mushy zone and the outside bath is balanced by the mechanical pressure exerted by the stretching lens capsule due to the presence of a distinct water front [40].
- The osmotic pressure difference between the core and the outside bath drives water penetration and thus expansion of the mushy zone, which continues until the osmotic pressure is balanced by the mechanical pressure from the stretched lens capsule.
- The bath concentration is constant, and unstirred layer effects are neglected.

- A pressure gradient cannot be supported within the lens, resulting in an equilibrated hydrostatic pressure between the mushy zone and core.

2.2.3 Computational Model

A complete derivation of the governing ODE is provided in Appendix B, and an explanation of variables is listed in Table 1:

$$\frac{dr}{dt} = \left(\frac{1}{L_p} + \frac{r - \sqrt[3]{\dfrac{r_0^3 - f(E,r,zc)r^3}{1 - f(E,r,zc)}}}{K_m} \right)^{-1} \left[2RT\left(\sqrt{m^2 + \frac{(zc)^2}{4}} - m \right) - \frac{2Eh}{r_0(1-\nu)}\left(1 - \frac{r_0}{r}\right) \right] \tag{1}$$

Table1: Governing Equation Variables

Parameter	Description	Value	Units	Reference
E	Modulus of elasticity	§	Pa	‡
h	Capsule thickness	Mouse $11.4x10^{-6}$	m	(Danysh et al., 2008) ‡
		Porcine $58x10^{-6}$		(Wollensak et al., 2004) ‡
K_m	Darcy Conductivity of mushy zone	§	$m^2 \bullet Pa^{-1} \bullet s^{-1}$	‡
L_p	Capsule hydraulic conductivity	Rat (used for Mouse) $4.8x10^{-11}$	$m \bullet Pa^{-1} \bullet s^{-1}$	(Fisher, 1988) ‡
		Porcine $7.5x10^{-11}$		(Fisher, 1977)
m	Concentration of bath solution	17.11* 51.33 85.56	mol• m^{-3}	0.1 % w/v* 0.3 % w/v 0.5 % w/v
r	Radius of the lens	†	m	†
r_0	Initial radius of lens	†	m	†
R	Universal gas constant	8.314	$m^3 \bullet Pa \bullet K^{-1}_1 \bullet mol^-$	----------
t	Time	†	s	†
T	Ambient temperature	293	K	----------
zc	Fixed charge density of lens fiber cells	§	mol• m^{-3}	(Bartels and Elliott, 1993) ‡
ν	Poisson's ratio	0.47	----------	(Fisher, 1969; Koretz and Handelman, 1982) ‡

* See Appendix C for unit conversion from % w/v to mol• m^{-3}
† Values measured during experiment
‡ See Appendix D for a discussion of the literature and fitted constants
§ Fitting parameter in the computational model

2.2.4 Data Processing

The numerical solution to Eq. (1) was obtained using the MATLAB *ode23s* routine and the parameter values listed in Table 1 (See Appendix A II, III, IV and VI for MATLAB code). Recognizing that the thickness of the lens capsule is not uniform [22,49,50], we take an average thickness h determined from the anterior surface of the porcine lens [51] and from the equatorial region of the mouse lens [49]. We investigate values of the fixed charge density zc within the range of 10 and 20 mM determined in bovine lens [46]. The values of the elastic modulus, E, and Darcy conductivity of mushy zone, K_m, were chosen to minimize the sum of squared error between the simulated and experimental r vs. t data using a MATLAB *fminsearch* routine. Peirce's criterion was used to evaluate the elastic modulus at each bath concentration [52].

3. RESULTS

Figure 4 depicts the results of representative experiments with their numerical solution to Eq. (1) for each NaCl bath concentration used with the porcine and mouse models. The symbols represent experimental data, and the solid lines represent the numerical solutions, with modulus of elasticity, E, and Darcy conductivity of the mushy zone, K_m, as fitting parameters for each data set independently; the fixed charge density, zc, was set at 20 mol·m^{-3}.

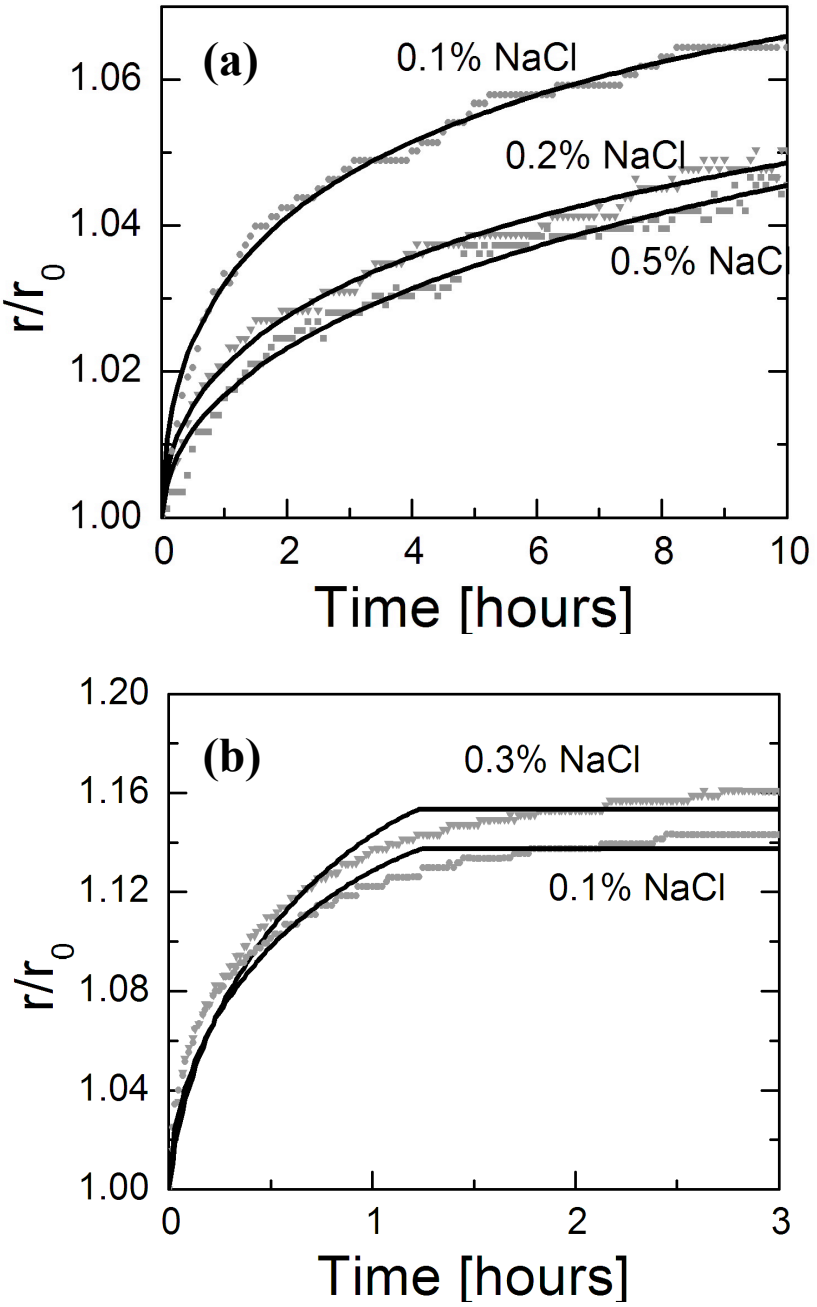

Figure 4: Computational model fitted to experimental data. Computational model (solid lines) fitted to experimental data (symbols) of lens expansion for the (a) porcine and (b) mouse models. Data are representative experiments from each bath concentration, with the fixed charge density, *zc*, set at 20 mol·m^{-3}. Discrete steps in the experimental data were caused by the limit of measurement resolution.

Typical sum-of-squared error (SSE) vs. E and K_m plots are given in Fig. 5. When E is increased and K_m decreased (or vice versa), the error rises rapidly, but if E and K_m both increase (or decrease), there is relatively little change in the error, as seen by the shallow trough in Fig. 5a and the highly elliptical contours in Fig. 4b. For a two-parameter model, a reasonable estimate of the 95% confidence ellipse on the fitted parameters is detailed in Appendix E. The data set used to generate figures 5 and 6 was from a porcine lens that contained 40 images (less than an image every 10 minutes); $SSE_{95\%}$=1.17 SSE_{min} [53]. The number of images was significantly increased for the mouse data sets, reducing the error confidence interval to $SSE_{95\%}$=1.034 SSE_{min} (Appendix E).

For the plots in Fig. 5, SSE_{min}=.00125, giving $SSE_{95\%}$=.00146. The axes of the confidence ellipse do not coincide with the E and K_m axes. The K_m that produced minimum error at each value of E was plotted against E (Fig. 6a), resulting in a nearly linear line with slope 1. This line plots the valley of the trough for the error contour graph in Fig. 4b. With an intercept of 0.2 and error determined from the 95% confidence ellipse, the rotated coordinates of the ellipse correspond to the following equations:

$E-K= -0.2 +/- .05E_{min}$, where E_{min} =2.38 MPa

$K-E= 0.2 +/- .26K_{min}$, where $K_{min}= 2.56 \times 10^{-16}$ $m^2 \cdot Pa^{-1} \cdot s^{-1}$

In Fig. 6b the value of error for each K_m and E combination in Fig. 6a is plotted against E. This is the same trough from figure 5a on a different scale. It demonstrates that the value obtained in from the processing code (E=2.4 MPa) is the value that globally generates the smallest SSE.

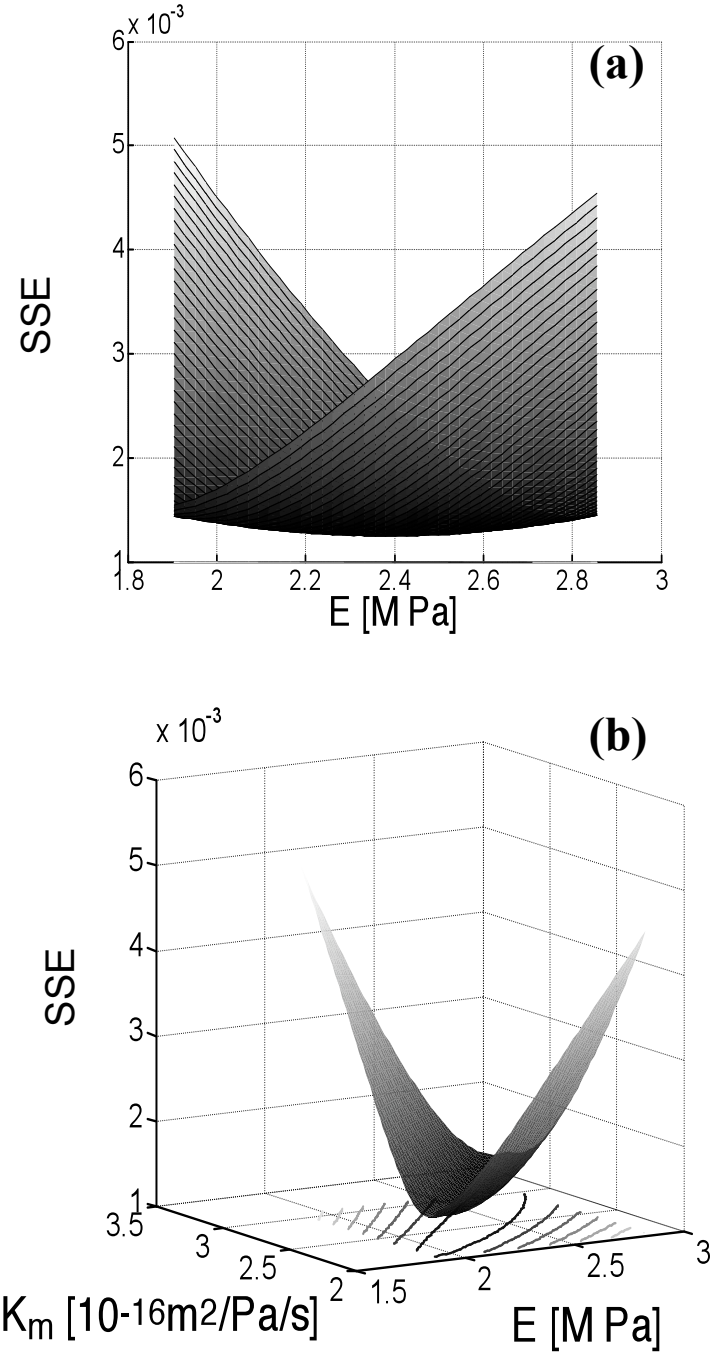

Figure 5: Contour of sum of squared error vs. capsule elastic modulus and mushy zone Darcy conductivity. Sum of squared error (SSE) (a) plotted vs. modulus of elasticity of the lens capsule, E, and (b) plotted vs. E and Darcy conductivity of the mushy zone, K_m. A shallow trough lies along the line $E = K_m + .02$, with units of MPa and 10^{-16} $m^2 \cdot Pa^{-1} \cdot s^{-1}$ for E and K_m respectively. Results are from a porcine lens in 0.1% NaCl bath and based on zc=20 $mol \cdot m^{-3}$.

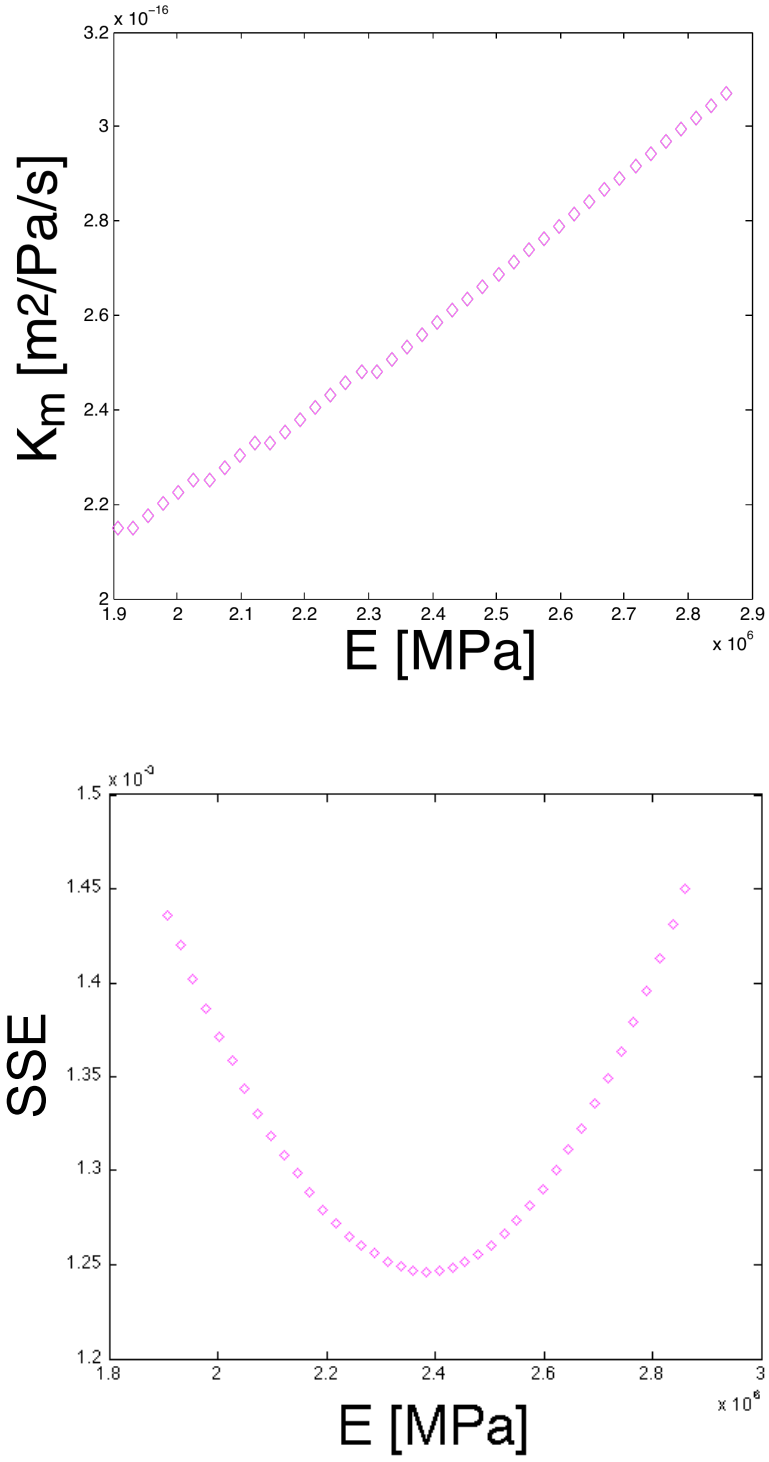

Figure 6: Graph of mushy zone Darcy conductivity and sum of squared error vs. capsule elastic modulus. (a) Darcy conductivity of the mushy zone that produced the minimum error at each value of *E,* plotted against *E*. (b) Sum of squared error for each K_m and *E* combination plotted against *E*.

As can be seen in Fig. 5b, the confidence ellipses have a long direction, yielding fairly large confidence intervals (roughly +/- 25%) when E and K_m are both allowed to vary. Thus we expect that the estimated values are within 25-30% of the true value. We observe that if E or K_m were known from some other measurement, the confidence intervals would be tightened considerably. For mouse data sets, when three hours of data is used in the computational model, the confidence interval is reduced to 10% of the estimated value.

3.1 Porcine

One data point was removed as an outlier from the 0.5% saline bath concentration dataset at zc=20 mol·m^{-3}. The average elastic modulus of the lens capsule at zc=20 mol·m^{-3} was 2.0±0.5 MPa (mean ± 95% confidence interval; n=15) for 0.1% saline solution, 0.64±0.3 MPa (n=10) for 0.2% saline solution, and 0.28±0.5 MPa (n=6) for 0.5% saline solution. For zc=10 mol·m^{-3}, the average elastic modulus was 0.58±0.1 MPa (n=15) for 0.1% saline solution, 0.20±0.08 MPa (n=10) for 0.2% saline solution, and 0.24±0.02 MPa (n=7) for 0.5% saline solution. The data are shown in Fig. 7 with reported literature values of the porcine lens elastic modulus for comparison. It is noted that the Krag and Andreasson value is a secant modulus at 10% uniaxial strain (calculated from table III [23]) and may not be directly comparable to our measurement, which is primarily biaxial.

The average initial radius of the lens was 4700±110μm (mean ± 95% confidence interval) n=12 for the experiments with 0.1% saline bath concentration, 4500±120 μm

n=9 for the 0.2% saline bath, and 4450±150 μm n=5 for the 0.5% saline bath. There was no significant difference among the initial lens radii of the three groups of experiments (p=0.38 by analysis of variance, ANOVA). Rotation of a single image (from -15º to 15º with 5º steps) and subsequent measurement of the equatorial diameter produced less than 1% error.

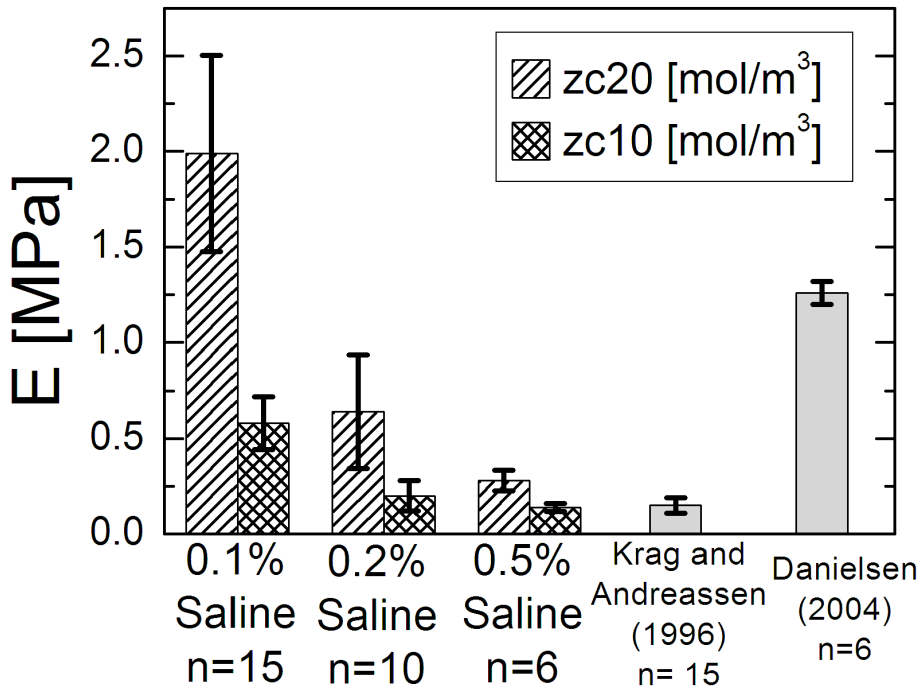

Figure 7: Porcine capsule elastic modulus experimental and literature values. Error bars are 95% confidence intervals.

3.1 Mouse

Twenty-one mice were tested: 11 at 0.3% and 10 at 0.1% saline solution. The genotypes were obtained after data collection and analysis; however, the distribution of Alport and wild type within each group was nearly the same. Among the lenses tested at 0.3% bath concentration, 4 were wild type and 7 were Alport. Among the lenses tested at 0.1% bath concentration, 3 were wild type and 7 were Alport. The modulus of elasticity and the hydraulic conductivity of the mushy zone were determined from the computational model for each data set using one, two, and three hours of data. Reported here are the elastic moduli for one and two hours of equatorial data and two hours of sagittal data, and the hydraulic conductivity for two hours of equatorial data.

Data sets were evaluated at a fixed charge density of 15 and 20 $mol \cdot m^{-3}$. The fit was poor at a fixed charge density of 10 $mol \cdot m^{-3}$, so the second value of 15 was chosen because the fit was significantly improved and within the 10- 20 $mol \cdot m^{-3}$range determined by Bartels and Elliott [46]. Equatorial and sagittal data were analyzed for outliers based on Peirce's criterion at both zc values in each category (0.1% WT, 0.3% WT, 0.1% Alport, 0.3% Alport). One set was removed from the equatorial and sagittal data at both fixed charge densities (the same data set) for 0.3% Alport and wild type and 0.1% Alport. Additionally, sagittal information was not obtained for two data sets from the Alport 0.1% and one data set from the 0.3% wild type. Due to camera malfunction, a portion of images were not captured in early data points for one experiment (WT 0.3%); the number of data points were not great enough to generate a fit at one hour of. data collection. Also, the error for zc=20 and zc=15 for one WT 0.3% data set and for zc=15

for one Alport 0.3% data were outliers, so they were not included in the analysis. Lastly, one data set was not used in the maximum strain at 3 hours and rupture analysis from the Alport 0.1% concentration because a bubble was developed that prevented accurate determination of the equatorial diameter. However, at 2 hours the strain was 16% and the lens did not rupture within 4 hours. The number of data sets, n, is provided for each graph since data exclusion varies with the parameters being investigated, as outlined above.

The average initial equatorial radius was 1150±17μm (mean ± 95% confidence interval, n=12) for Alport lenses and 1152 ±23μm (n=7) for wild type lenses. The average initial sagittal radius was 963 ±23μm (n=12) for Alport lenses and 937 ±22μm (n=7) for wild type lenses.

The average values of elastic modulus and hydraulic conductivity are shown in Fig. 8 and 9, respectively, using two hours of data for the computational model. The modulus of elasticity measured by Danielsen for the rat [27] is included in Fig. 8 for comparison.

The average elastic modulus of the lens capsule at zc=20 $mol \cdot m^{-3}$ was 1.8±0.3 MPa (mean ± 95% confidence interval; n=3) for WT and 1.4±0.2 MPa (n=6) for Alport lenses in 0.1% saline solution, and 0.43±0.01 MPa (n=3) for WT and 0.5±0.1 MPa (n=6) for Alport lenses in 0.3% saline solution. For zc=15 $mol \cdot m^{-3}$, the average elastic modulus was 1.0±0.2 MPa (n=3) for WT and 0.8±0.1 MPa (n=6) for Alport lenses in 0.1% saline solution, and 0.25 MPa (n=1) for WT and 0.29±0.06 MPa (n=6) for Alport lenses in 0.3% saline solution.

The average Darcy conductivity of the mushy zone at zc=20 $mol \cdot m^{-3}$ was 0.7±0.3 $m^2 \cdot Pa^{-1} \cdot s^{-1}$ (n=3) for WT and 0.8±0.2 $m^2 \cdot Pa^{-1} \cdot s^{-1}$ (n=7) for Alport lenses in 0.1% saline solution, and 2.4±0.4 $m^2 \cdot Pa^{-1} \cdot s^{-1}$ (n=2) for WT and 2.3±0.4 $m^2 \cdot Pa^{-1} \cdot s^{-1}$ (n=6) for Alport lenses in 0.3% saline solution. For zc=15 $mol \cdot m^{-3}$, the average Darcy conductivity was 1.4±0.7 $m^2 \cdot Pa^{-1} \cdot s^{-1}$ (n=3) for WT and 1.5±0.5 $m^2 \cdot Pa^{-1} \cdot s^{-1}$ (n=7) for Alport lenses in 0.1% saline solution, and 6±1 $m^2 \cdot Pa^{-1} \cdot s^{-1}$ (n=2) for WT and 7±1 $m^2 \cdot Pa^{-1} \cdot s^{-1}$ (n=6) for Alport lenses in 0.3% saline solution.

The average elastic modulus determined by the computational model using one hour of data is shown in Fig. 10. The elastic modulus determined by the computational model using two hours of sagittal strain data is shown in Fig. 11. On average, the strain reached by the sagittal and equatorial diameters in 3 hours were similar in Alport and wild type lenses regardless of bath concentration (Fig. 12). These data do not include lenses that ruptured before 3 hours. When individual data sets are plotted, however, a statistically significant trend is observed (Fig. 13). Wild type (2/2) and Alport (5/5) lenses that strained less than 14% all survived. Lenses that strained greater than 14% had a higher tendency to rupture if they were Alport (7/8 in comparison to 1/5 for WT; p=0.03, Chi Square- Test). Images of a lens before and after capsule rupture are shown in Fig 14.

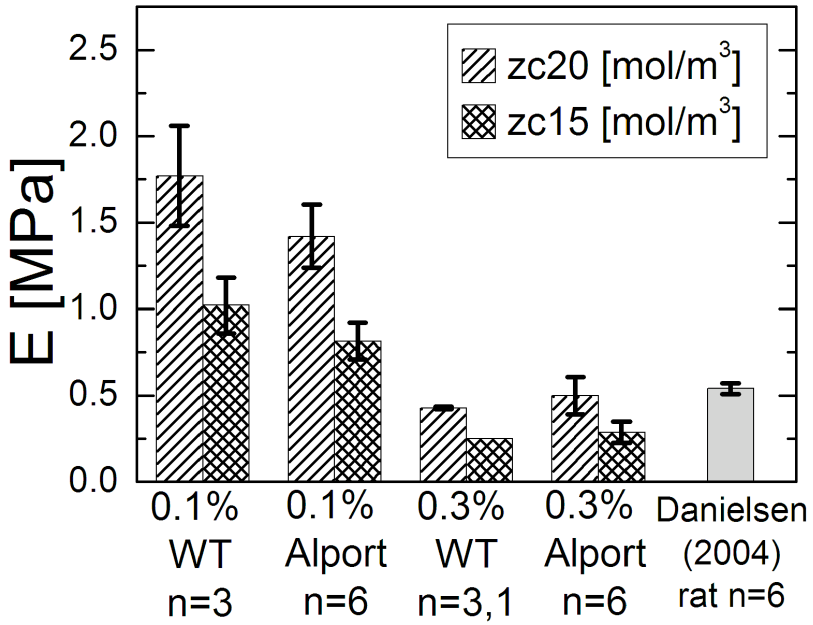

Figure 8: Mouse capsule elastic modulus experimental and literature values using 2 hours of data. Error bars are 95% confidence intervals.

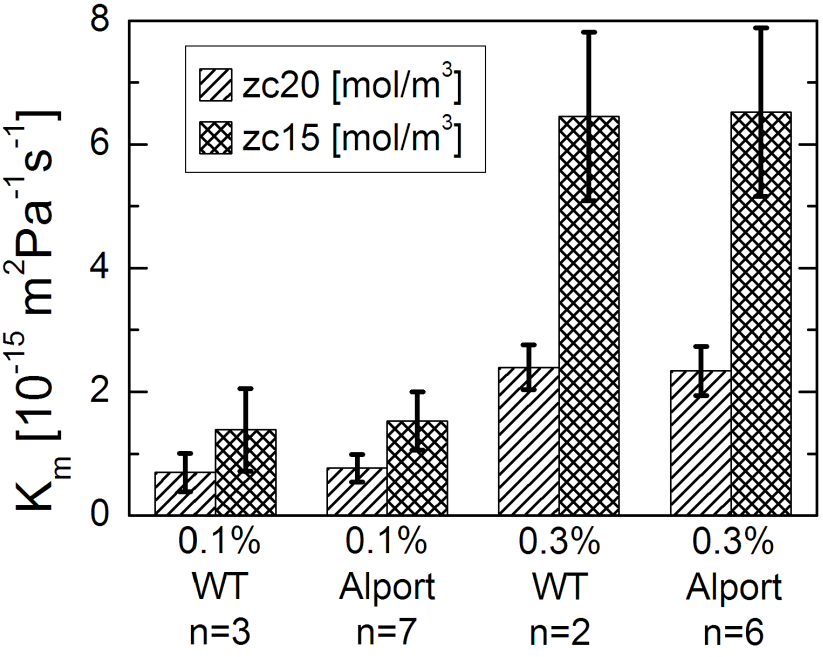

Figure 9: Mouse mushy zone Darcy conductivity experimental values using 2 hours of data. Error bars are 95% confidence intervals.

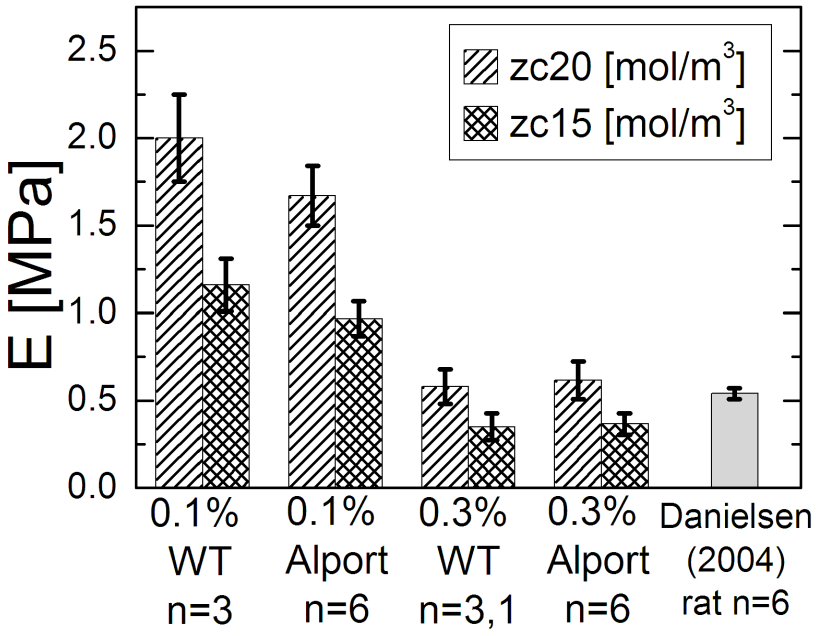

Figure 10: Mouse capsule elastic modulus experimental and literature values using 1 hour of data: Error bars are 95% confidence intervals.

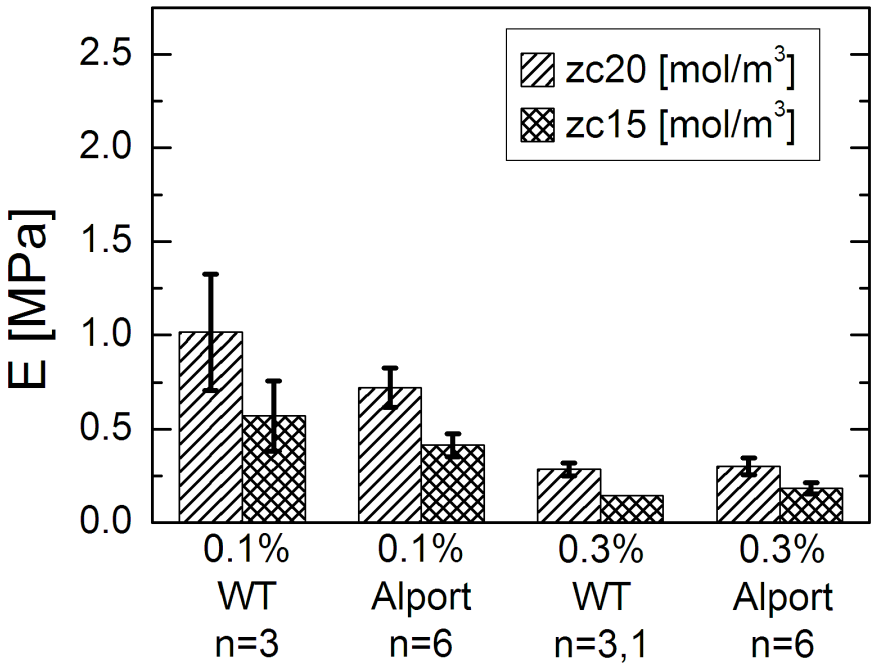

Figure 11: Mouse capsule elastic modulus experimental and literature values using 2 hours of sagittal radius strain data: Error bars are 95% confidence intervals.

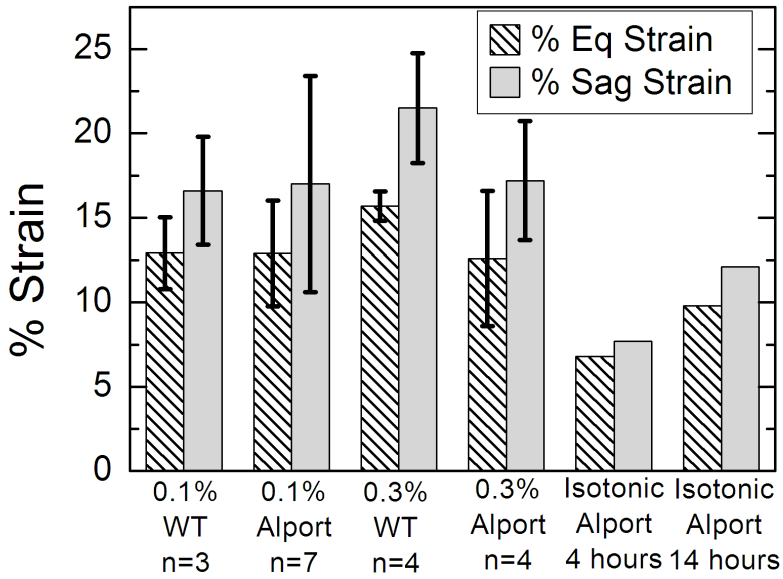

Figure 12: Mouse lens radial strain after 3 hours in hypotonic solution. Two lenses placed in physiologically isotonic solution for 4 and 14 hours are also included. Error bars are 95% confidence intervals.

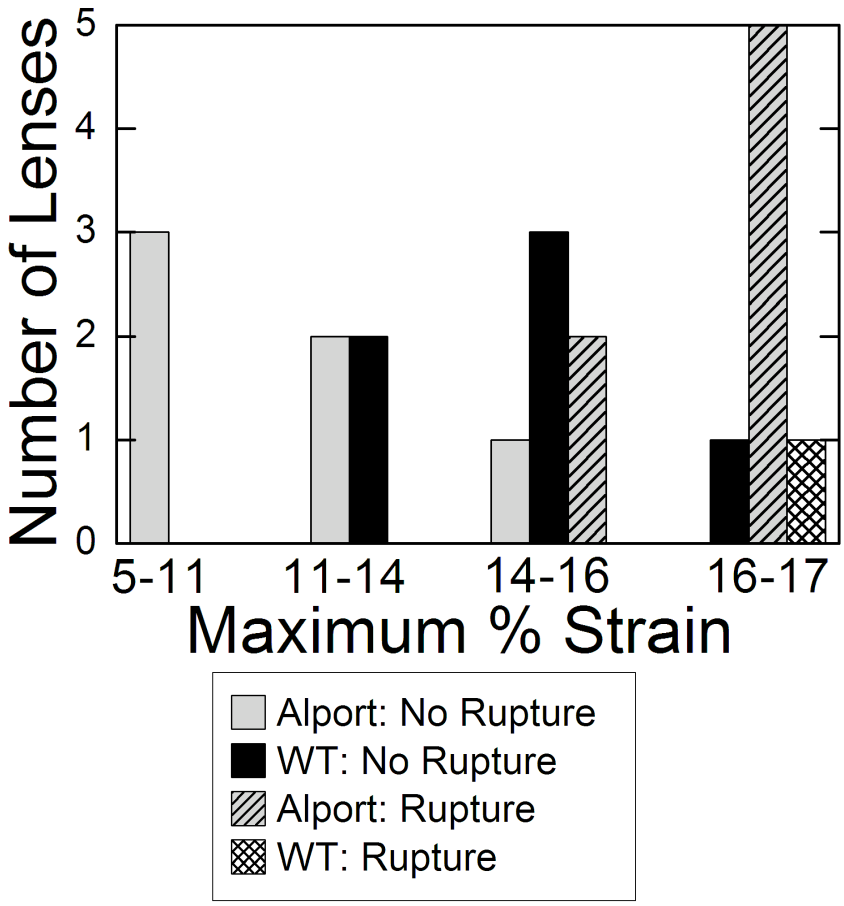

Figure 13: Mouse lens strain before rupture or after 4 hours in hypotonic solution.

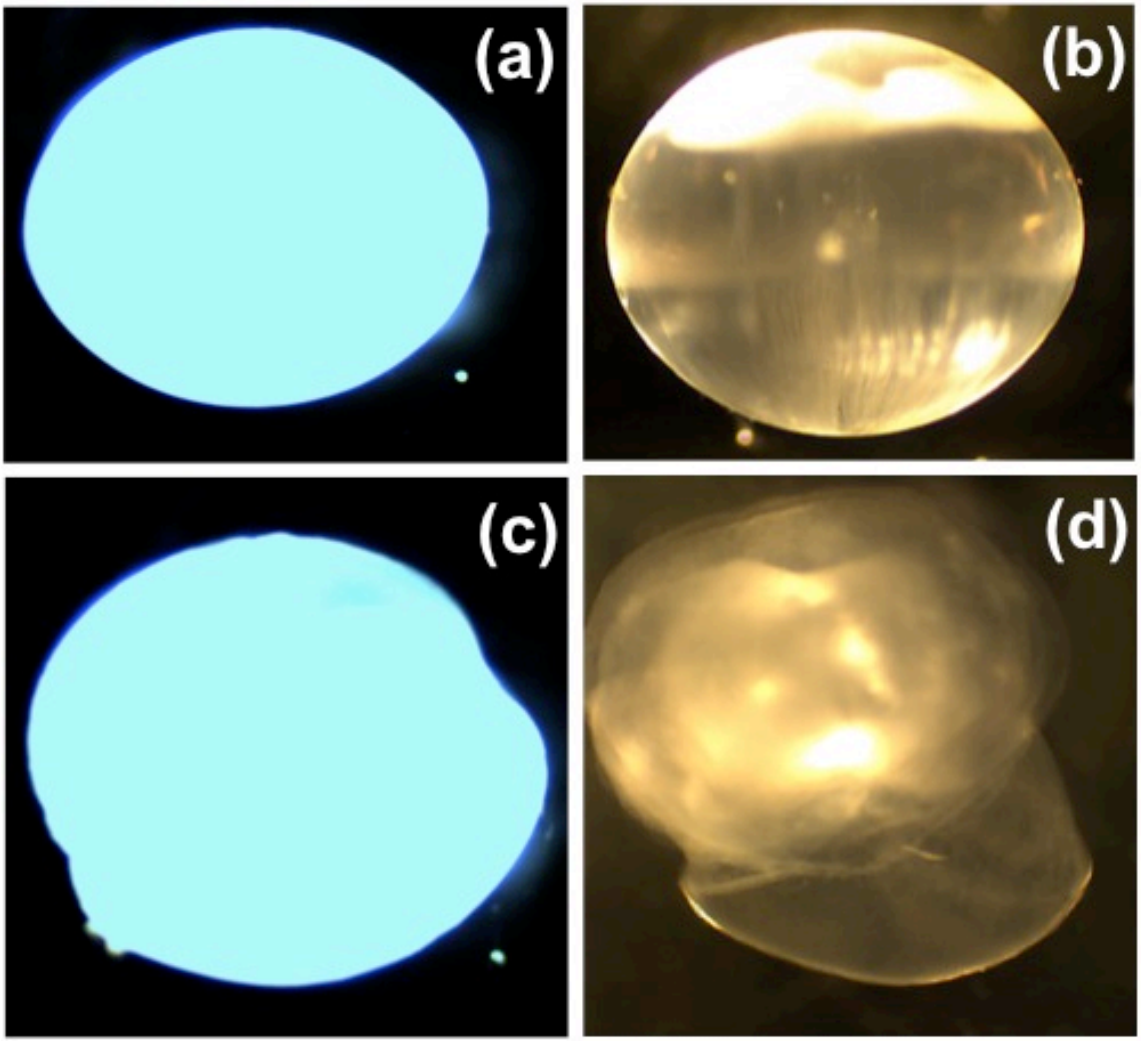

Figure 14: Mouse capsule rupture images. Mouse lens (a, b) before and (c, d) after lens capsule rupture with different light source intensities. Images (a) and (c) are from a different experiment than images (b) and (d).

4. DISCUSSION

4.1 Porcine

The osmotic swelling method developed with the porcine model provides a quantitative assessment of the lens capsule modulus of elasticity without requiring dissection of the capsule. Unlike traditional mechanical techniques, the minimal manipulation allows osmotic swelling to be extended to small animal models such as the mouse. The elastic modulus estimates are made at small strains (<10%), which are physiologically relevant, as this is where accommodation occurs [22].

The elastic modulus determined through the osmotic swelling model is comparable to previously reported values. The secant modulus calculated from Table III of Krag and Andreassen [23] was obtained from uniaxial extension tests of pre-strained capsule rings while the elastic modulus calculated by our model and by Danielsen [27], who utilized Fisher's biaxial method of inflation [25], came from multiaxial extension tests. Although the elastic modulus from Krag and Andreassen shown in Fig. 5 is calculated from pre-strained capsular rings, the alignment of the fibers is still likely to affect the apparent elastic modulus. Under uniaxial loading, the collagen IV network initially straightens in the low strain region (<10%). Under biaxial loads, however, the collagen IV network does not experience the initial straightening [18]. X-ray diffraction has shown networks of randomly oriented collagen fibers in unstretched, air-dried bovine lens capsules and has demonstrated the reorientation of fibers parallel to the direction of applied stress in stretched collagen networks [54]. The effect of loading type has been shown with the human lens capsule. Fisher [25] reported values of 3-6 MPa using inflation, as compared to 0.4-1.5 MPa measured by Krag et al. [55] using uniaxial ring-pulling. Therefore, the

higher modulus observed by our model and Danielson as compared to Krag and Andreassen is expected.

Our data show an increase in measured modulus with hypotonicity, especially when a higher estimated value for zc is used. This increase is inconsistent with our assumption of a linear material and must therefore be examined in more depth. The obvious explanation would be that the mechanical response is nonlinear, as observed by Krag and Andreassen [23] and consistent with some combination of material nonlinearity of the type IV collagen triple helix and kinematic nonlinearity due to rearrangement of the collagen network. Another important consideration is that the numerous simplifications made in deriving the model may lead to inaccurate but reproducible estimates of the lens capsule properties. The following paragraphs discuss potential sources of error from the model.

The simplification of the transport and thermodynamics within the lens to a lumped, well-mixed system containing only fixed charge and monovalent ions was made to simplify analysis of the data and minimize the number of empirical parameters, but it could lead to incorrect results. The validity of the lumped model can be assessed by calculating the characteristic diffusion time. For small ions, the diffusion coefficient is expected to be on the order of 0.001 $mm^2 \cdot s^{-1}$ [48]. Early in the experiment, the mushy zone is relatively thin (~ 0.5 mm at t ~ 2 hours), and the diffusion time scale is short (~ 5 min). At the end of the experiment, the mushy zone thickness is approximately 1.5 mm, which corresponds to a diffusion time scale of 40 min, which is rapid compared to the 10-hr experiment but long enough to be an issue.

In light of this concern, the following analysis is made. Since the volume change is not very large (~20% for 7% radial expansion), the chemical environment within the lens (i.e., the osmotic pressure driving water into the lens) does not change dramatically during the experiment. An increase in elastic modulus, E, reduces the equilibrium expansion of the lens, shifting the radius vs. time curve down. An increase in permeability of the mushy zone, K_m, allows the system to equilibrate more quickly due to increased water mobility, shifting the radius vs. time curve to the left. Thus, the net effect of the combined increases in E and K_m is small, as seen in Figure 4. It would be possible to separate the two parameters more effectively if the experiment were run to equilibrium, but we found that the tissue began to deteriorate after 10 hours, so we were not able to explore longer times. For a smaller lens, the equilibration time might be faster, so the method may work better in, e.g., the mouse.

The value of the fixed charge density zc was held constant, and two values were analyzed. Since our goal is to quantify the change in the elastic modulus as the composition of the basement membrane is altered through genetic manipulation, this model is appropriate for the intended use regardless of the chosen zc. It is observed, however, that an accurate measurement of the elastic modulus cannot be determined without knowing the value of the fixed charge density. Even if the fixed charge density were known, the electrochemistry of the lens is assuredly more subtle than a collection of only fixed charges and monovalent ions. We therefore reiterate that the modulus values calculated from our analysis of a swelling experiment are better suited to comparison between different lens capsules than to specific quantitative application. If more

information about the charged species and the transport properties within the lens were to become available, a distributed model following those of Ateshian [56] and Haider [57] could be developed. Heistand et al. [7] have developed a novel method of determining multiaxial mechanical behavior of the lens capsule. While their protocol can be used to determine more accurate and regional measurements of the modulus of elasticity, it is difficult to extend to the mouse lens due to its size.

There are many aspects of lens geometry and properties that are not captured by the approach we describe. These include variation in radius of curvature [58], capsule thickness [50], and collagen content [59] from the anterior to the posterior of the lens. For the mouse model, the lens was mounted so that the sagittal plane was imaged, which allowed for the measurement of both the equatorial and sagittal diameters. It is also noted that no evidence of active volume control [60] was observed, most likely due to the lack of energy source and low temperature.

In spite of the concerns raised here, osmotic swelling has the potential to quantify changes in lens capsule mechanical properties in the mouse lens, providing access to the genetic manipulability of the mouse. Traditional test methods [7,23,25] require isolation and manipulation of the sample that will be complicated, if not impossible, to achieve with the mouse lens. Atomic force microscopy (AFM) has recently been applied to the mouse lens capsule basement membrane [29], but AFM involves more difficult isolation and a highly complex deformation (involving compression, tension, shear, and finite-thickness effects simultaneously). Osmotic swelling offers a simpler approach, and this

preliminary study suggests that it is a feasible method to assess prefailure lens capsule elasticity at small strains (<10%).

4.2 Mouse

The maximum strain reached by the mouse lenses was significantly greater than the strain experienced by the porcine lenses. As a result, the computational model used the entire capacity of the core for swelling the mouse lens but did not completely use the core for the porcine lenses. A restriction had to be placed on the code that terminated swelling when the core was completely used, resulting in a sharp corner in the graph (Figure 4b). The elastic modulus was calculated based on an input of 1 (Fig. 10), 2 (Fig 8), and 3 hours of data. For each category, the elastic moduli obtained using different inputs were similar. The values of elastic modulus show the same pattern observed with the porcine lenses, increasing with an increase in hypotonicity or fixed charge density. Although Fig. 4b suggests that the full consumption of the core occurs after one hour of swelling, the corner in the graph was not eliminated when one hour of data was used.

Unlike the porcine swelling (Figure 4a), the mouse lenses swelled at the same rate in 0.1% and 0.3% NaCl w/v bath solutions (Figure 4b). This, along with the high rate of swelling, suggests that water transport may be limiting the rate of swelling. One potential consequence is that the free ions may not be able to leave the lens in the manner assumed by the model. Resultantly, the elasticity of the mouse lens capsule measured with this experimental data may not be appropriate due to the models inability to capture the complexity of a strong driving force. For future work, a solution of higher concentration will be used to decrease the osmotic driving force and rate of swelling. This may reduce

the water transport effects on the model, allowing the computational model to more accurately measure the modulus of elasticity.

The elasticity of the lens capsule measured in this work is not significantly different between the Alport and wild type mouse lenses in all bath concentrations using equatorial and sagittal strain data. Currently the same literature values needed for the computation model are being used for analysis of wild-type and Alport data. However, the capsule thickness and hydraulic conductivity may be affected by Alport syndrome. In related future work, the hydraulic conductivity will be measured for the wild type and Alport mouse lens capsule. Although the thickness of the lens capsule will not be measured, a hydroxyproline assay will be performed using the lens capsule to determine if the protein content is changing. This will show if the mass of the lens capsule is changing and provide insight into whether the capsule thickness may be changing. The Poisson's ratio should not be affected by Alport syndrome, because incompressibility is an intrinsic property of the fibers.

The strain in the sagittal plane is greater than the strain in the equatorial plane (Fig. 12), leading to a smaller value of elastic modulus when used in the computational model (Fig. 11). In future work, the sagittal information will used to obtain an estimate on the error associated with the assumption of the lens being a spherical shell. The average values of elasticity vary at most by a factor of two. With the assumptions used by the model and considering the model to be a comparative tool, the use of the equatorial radius should not affect the conclusions drawn from equatorial data. Also, it should be noted that the sagittal radii are not as accurate as the equatorial radii. The lens is

balanced on a round surface along its equator, and if the equatorial plane is not orthogonal to the plane of imaging, the apparent sagittal radius will appear larger than the actual sagittal radius. Although the lens does not move after it is placed, the angle may vary between the initial image captured in isotonic solution and the images captured while in the hypotonic bath, leading to inaccurate values of sagittal strain.

Figure 12 demonstrates that the lens swells in physiological isotonic solution (0.9% w/v). When the lenses are removed from the animal and placed in solution without an energy source, the ion pumps cannot maintain the physiological ion concentration. The rate of the resulting swelling is much less than the rate of swelling of lenses in 0.1% and 0.3% solutions; at 14 hours the lens has not reached the level of strain that lenses in the other solutions on average reach in 4 hours. This again suggests that a bath concentration closer to 0.9% w/v will have a lower rate of swelling, which may allow the model to more accurately determine the elasticity of the lens capsule and mushy zone Darcy hydraulic conductivity.

The phenomenon of lens capsule rupture was noticed while analyzing data sets. The lens capsule appears to undergo catastrophic failure during rupture (Fig 14). Images A and C were captured one minute apart during an experiment. The light source was adjusted in image B and D for visualization of lens details. Image C is an initial image of a lens before placement in hypotonic solution. Image D is an image taken a few minutes after the capsule ruptured. The mechanisms of basement membrane failure will be addressed in future experiments.

REFERENCES

1. Ruben GC, Yurchenco PD. High resolution platinum-carbon replication of freeze-dried basement membrane. Microsc Res Tech 1994; 28:13-28.

2. Barnard K, Gathercole LJ. Short and long range order in basement membrane type IV collagen revealed by enzymic and chemical extraction. Int J Biol Macromol 1991; 13:359-65.

3. Kelley PB, Sado Y, Duncan MK. Collagen IV in the developing lens capsule. Matrix Biol 2002; 21:415-23.

4. Fisher RF. The deformation matrix theory of basement membrane: a study of water flow through elastic and rigid filaments in the rat. J Physiol 1988; 406:1-14.

5. Sundaramoorthy M, Meiyappan M, Todd P, Hudson BG. Crystal structure of NC1 domains. Structural basis for type IV collagen assembly in basement membranes. J Biol Chem 2002; 277:31142-53.

6. Donaldson P, Kistler J, Mathias RT. Molecular solutions to mammalian lens transparency. News Physiol Sci 2001; 16:118-23.

7. Heistand MR, Pedrigi RM, Delange SL, Dziezyc J, Humphrey JD. Multiaxial mechanical behavior of the porcine anterior lens capsule. Biomech Model Mechanobiol 2005; 4:168-177.

8. Gerometta R, Zamudio AC, Escobar DP, Candia OA. Volume change of the ocular lens during accommodation. Am J Physiol Cell Physiol 2007; 293:C797-804.

9. Burd HJ, Judge SJ, Cross JA. Numerical modelling of the accommodating lens. Vision Res 2002; 42:2235-251.

10. Colville DJ, Savige J. Alport syndrome. A review of the ocular manifestations. Ophthalmic Genet 1997; 18:161-73.

11. Fisher RF. Changes in the permeability of the lens capsule in senile cataract. Trans Ophthalmol Soc U K 1977; 97:100-3.

12. Bredrup C, Matejas V, Barrow M et al. Ophthalmological aspects of Pierson syndrome. Am J Ophthalmol 2008; 146:602-611.

13. Peczon BD, Peczon JD, Cintron C, Hudson BG. Changes in chemical composition of anterior lens capsules of cataractous human eyes as a function of age. Exp Eye Res 1980; 30:155-65.

14. Pirie A. Difference in swelling and opacity formation between young and old lenses. Nature 1967; 216:503-504.

15. LeBleu VS, Macdonald B, Kalluri R. Structure and function of basement membranes. Exp Biol Med (Maywood) 2007; 232:1121-1129.

16. Miosge N. The ultrastructural composition of basement membranes in vivo. Histol Histopathol 2001; 16:1239-1248.

17. Kalluri R. Basement membranes: structure, assembly and role in tumour angiogenesis. Nat Rev Cancer 2003; 3:422-33.

18. Danysh BP, Duncan MK. The lens capsule. Exp Eye Res 2009; 88:151-164.

19. Hassell J, Yamada Y, Arikawa-Hirasawa E. Role of perlecan in skeletal development and diseases. Glycoconj J 2002; 19:263-267.

20. Yan Q, Clark JI, Wight TN, Sage EH. Alterations in the lens capsule contribute to cataractogenesis in SPARC-null mice. J Cell Sci 2002; 115:2747-2756.

21. Rheault MN, Kren SM, Thielen BK et al. Mouse model of X-linked Alport syndrome. J Am Soc Nephrol 2004; 15:1466-1474.

22. Krag S, Andreassen TT. Mechanical properties of the human lens capsule. Prog Retin Eye Res 2003; 22:749-767.

23. Krag S, Andreassen TT. Biomechanical measurements of the porcine lens capsule. Exp Eye Res 1996; 62:253-260.

24. Krag S, Andreassen TT. Mechanical properties of the human posterior lens capsule. Invest Ophthalmol Vis Sci 2003; 44:691-696.

25. Fisher RF. Elastic constants of the human lens capsule. J Physiol 1969; 201:1-19.

26. Fisher RF, Hayes BP. Thickness and volume constants and ultrastructural organization of basement membrane (lens capsule). J Physiol 1979; 293:229-245.

27. Danielsen CC. Tensile mechanical and creep properties of Descemet's membrane and lens capsule. Exp Eye Res 2004; 79:343-350.

28. David G, Pedrigi RM, Heistand MR, Humphrey JD. Regional multiaxial mechanical properties of the porcine anterior lens capsule. J Biomech Eng 2007; 129:97-104.

29. Candiello J, Balasubramani M, Schreiber EM et al. Biomechanical properties of native basement membranes. FEBS J 2007; 274:2897-2908.

30. Mela MJ. Elastic-Mathematical Theory of Cells and Mitochondria in Swelling Process: The Membranous Stresses and Modulus of Elasticity of the Egg Cell of Sea Urchin, Strongylocentrotus purpuratus. Biophys J 1967; 7:95.

31. Mlekoday H. Osmotic water permeability of the human red cell. Dependence on direction of water flow and cell volume. J Gen Physiol 1983; 81:213-220.

32. Cosgrove D. Biophysical Control of Plant Cell Growth. Annual Reviews in Plant Physiology 1986; 37:377-405.

33. Wolfe J, Dowgert MF, Steponkus PL. Mechanical study of the deformation and rupture of the plasma membranes of protoplasts during osmotic expansions. J Membr Biol 1986; 93:63-74.

34. Zimmermann U, Steudle E. The pressure-dependence of the hydraulic conductivity, the membrane resistance and membrane potential during turgor pressure regulation in Valonia utricularis. J Membr Biol 1974; 16:331-352.

35. Philip JR. The Osmotic Cell, Solute Diffusibility, and the Plant Water Economy. Plant Physiol 1958; 33:264-271.

36. Cotlier E, Kwan B, Beaty C. The lens as an osmometer and the effects of medium osmolarity on water transport, 86Rb efflux and 86Rb transport by the lens. Biochim Biophys Acta 1968; 150:705-722.

37. Jacob TJ, Duncan G. Osmotic influences on lens membrane characteristics. Exp Eye Res 1980; 31:505-512.

38. Patterson JW, Fournier DJ. The effect of tonicity on lens volume. Invest Ophthalmol 1976; 15:866-869.

39. Wang H, Gao J, Sun X et al. The Effects of GPX-1 Knockout on Membrane Transport and Intracellular Homeostasis in the Lens. J Membr Biol 2009; 227:25-37.

40. Young MA, Tunstall MJ, Kistler J, Donaldson PJ. Blocking chloride channels in the rat lens: localized changes in tissue hydration support the existence of a circulating chloride flux. Invest Ophthalmol Vis Sci 2000; 41:3049-3055.

41. Crank J. The Mathematics of Diffusion. Oxford, Eng: Clarendon Press, 1975; 414.

42. Fowler AC, Krantz WB. A Generalized Secondary Frost Heave Model. SIAM J Appl Math 1994; 54:1650-1675.

43. Fedors RF. Osmotic effects in water absorption by polymers. Polymer 1980; 21:207-212.

44. Gere JM, Goodno BJ. Spherical Pressure Vessels. In: Mechanics of Materials. Toronto ON, Canada: Cengage Learning, 2009;621-626.

45. Kedem O, Katchalsky A. Thermodynamic analysis of the permeability of biological membranes to non-electrolytes. 1958. Biochim Biophys Acta 1989; 1000:413-430.

46. Bartels EM, Elliott GF. The effect of ATP on the Donnan potential and protein fixed charge in bovine lens fibres. Journal of Physiology-London then Cambridge 1993; 467:279P.

47. Plonsey R, Roger CB. Donnan Equilibrium. In: Bioelectricity: A Quantitative Approach. New York: Plenum Press, 1988;44-47.

48. Paterson CA. Distribution and movement of ions in the ocular lens. Doc Ophthalmol 1972; 31:1-28.

49. Danysh BP, Czymmek KJ, Olurin PT, Sivak JG, Duncan MK. Contributions of mouse genetic background and age on anterior lens capsule thickness. Anat Rec (Hoboken) 2008; 291:1619-1627.

50. Barraquer RI, Michael R, Abreu R, Lamarca J, Tresserra F. Human lens capsule thickness as a function of age and location along the sagittal lens perimeter. Invest Ophthalmol Vis Sci 2006; 47:2053-2060.

51. Wollensak G, Sporl E, Pham DT. Biomechanical changes in the anterior lens capsule after trypan blue staining. J Cataract Refract Surg 2004; 30:1526-1530.

52. Ross SM. Peirce's criterion for the elimination of suspect experimental data. J Eng Tech 2003:38-41.

53. Draper NR, Smith H. Applied Regression Analysis. New York: Wiley, 1981; 709.

54. Roveri N, Ripamonti A, Bigi A, Volpin D, Giro MG. X-ray diffraction study of bovine lens capsule collagen. Biochim Biophys Acta 1979; 576:404-408.

55. Krag S, Olsen T, Andreassen TT. Elastic properties of the lens capsule in relation to accommodation. Invest Ophthalmol Vis Sci 1996; 37:774.

56. Ateshian GA, Likhitpanichkul M, Hung CT. A mixture theory analysis for passive transport in osmotic loading of cells. J Biomech 2006; 39:464-475.

57. Haider MA, Schugart RC, Setton LA, Guilak F. A mechano-chemical model for the passive swelling response of an isolated chondron under osmotic loading. Biomech Model Mechanobiol 2006; 5:160-171.

58. Heistand MR, Pedrigi RM, Dziezyc J, Humphrey JD. Redistribution of strain and curvature in the porcine anterior lens capsule following a continuous circular capsulorhexis. J Biomech 2006; 39:1537-1542.

59. Fitch J, Mayne R, Linsenmayer T. Developmental acquisition of basement membrane heterogeneity: type IV collagen in the avian lens capsule. J Cell Biol 1983; 97:940.

60. Zhang JJ, Jacob TJ. Volume regulation in the bovine lens and cataract. The involvement of chloride channels. J Clin Invest 1996; 97:971-978.

61. Koretz JF, Handelman GH. Model of the accommodative mechanism in the human eye. Vision Res 1982; 22:917-927.

62. Patterson CA, Delamere NA. The lens. In: Adler's physiology of the eye. St. Louis: Mosby-Year Book, 1992;348-390.

63. Lachish U. Osmosis and thermodynamics. American Journal of Physics 2007; 75:997.

64. Varadaraj K, Kumari S, Shiels A, Mathias RT. Regulation of aquaporin water permeability in the lens. Invest Ophthalmol Vis Sci 2005; 46:1393-1402.

65. Friedenwald JS. The Permeability of the Lens Capsule to Water, Dextrose, and Other Sugars. Trans Am Ophthalmol Soc 1930; 28:195-211.

66. Fisher RF. The influence of age on some ocular basement membranes. Eye 1987; 1 (Pt 2):184-189.

APPENDIX A: MATLAB Code

A. I. get_time_radius_TAP

```
function [u,t] = get_time_radius_TAP

%%Function measures and outputs the equatorial and sagittal radius for
%%all images of a data set and exports them into an output file:
%%output.TAP. Open with a text editor, copy and paste into an xcel
%%spreadsheet, or copy directly into data.TAP for analysis with
%%swelling_final_plot_TAP. Set variables at the beginning of this
%%function and swelling_final_plot_TAP.

%%%%%%%%%%%%%%%%%%%%%%%%%%%%%%%%%%
%% Variables to set for each data set
%%%%%%%%%%%%%%%%%%%%%%%%%%%%%%%%%%

name='5-02-10_malpm27_03c_'; %Image names within folder; all must be in
                             the same folder; number.tiff follows the dash
total=105;                  %Number extension of last image to be analyzed
offset=10;                   %The offset for the later pictures- ex) if
                             picture_7.tiff is taken at 4 min, it is the
                             5th picture (includes initial image); offset
                             is 2


%%%%%%%%%%%%%%%%%%%%%%%%%%%%%%%%%%
%% Loop for reading in images
%%%%%%%%%%%%%%%%%%%%%%%%%%%%%%%%%%
max=total-offset;            %actual number of images analyzed
i=1;
check_var3=1;

while i<max+1
    if check_var3==1
        question= 'Do you have another file?'; %%need to select initial
                             image and image at time 1- may need to select
                             more depending on first couple images
        button= questdlg(question,'Request to
continue','Yes','No','Yes');
        switch button
            case 'Yes'

                [filename,pathname] =uigetfile('*.*');
                             %manually select file

            case 'No'
                check_var3=0;
                m=i+offset;
                m=num2str(m);
                datafile_str=strcat(name,m,'.tiff');
                filename=  sprintf(datafile_str);
        end

    else
```

```
        m=i+offset;
        m=num2str(m);
        datafile_str=strcat(name,m,'.tiff');
                        %sets path for import of remaining images
                        through "max"
        filename=  sprintf(datafile_str);

    end
    f= imread(fullfile(pathname,filename));
                        %reads in file to be an image

%%%%%%%%%%%%%%%%%%%%%%%%%%%%%%%%%%
%% Image Adjustments and image conversion to grayscale and then black
%% and white
%%%%%%%%%%%%%%%%%%%%%%%%%%%%%%%%%%

%%Loop for rotating images- since initial image taken at a different
%%time, rotation is set up separately. Other images can also be rotated
%%separately.
    if i==1
        f=imrotate(f,-1);           %negative is clockwise
             elseif i==2 || i==3    %rotate image 2 and 3, 3 degrees
                                    clockwise
                f=imrotate(f,-3);
             elseif i==4 %f=imrotate(f,5); %rotate image 4, 5 degrees
                        counter clockwise

    else
        f=imrotate(f,-5);     %rotate all other images 5 degrees
                        clockwise
    end


    I=rgb2gray(f);            % Convert image to grayscale

%%Bubbles may need to be blacked out if they are too large and cannot
%%be eliminated in the "junk removal" below
%     I(1:200,1:100)=0; %Black out selected area; top left corner 0,0;
%     bottom right corner 768, 1024
%     I(1:100,:)=0;


    %imshow(I); %show gray-scale image on screen

    if i==1  % Establish the treshhold of gray scale for the first file
                        for BW conversion
        t=graythresh(I);
        tr=t*1.2;
        BW=im2bw(I,tr);
        check_var = 1;
        while check_var > 0;
            imshow(BW);
            title_str=strcat('\fontsize {14} Thresh = ', num2str(tr));
            title(title_str);
            button2= questdlg('Do you want to change Treshold','Request
                        to change','+','-','NO','N0');
```

```
            if button2 == '+'
                tr=tr+0.01;
                BW=im2bw(I,tr);
            elseif button2 == '--'
                tr=tr-0.01;
                BW=im2bw(I,tr);
            else
                check_var=0;
            end
        end

%%Junk Removal

        check_var2 = 1;
        disk=30;
        while check_var2 > 0;
            newBW=imopen(BW,strel('disk',disk));
            imshow(newBW);
            title_str2=strcat('\fontsize {14} Disk Elimination = ',
                              num2str(disk));
            title(title_str2);
            button3= questdlg('Do you want to change disk size
                              ','Request to change','+','-','NO','N0');

       %increment the size of disk until remove spheres of desired size

            if button3 == '+'
                disk=disk+2;
                BW=im2bw(I,tr);
                newBW=imopen(BW,strel('disk',disk)); %remove spheres
                          with a radius less than disk pixels
                imshow(newBW);
            elseif button3 == '--'
                disk=disk-2;
                BW=im2bw(I,tr);
                newBW=imopen(BW,strel('disk',disk)); %remove spheres
                          with a radius less than disk pixels
                imshow(newBW);
            else
                check_var2=0;
            end
        end

    else
        BW=im2bw(I,tr);
        newBW=imopen(BW,strel('disk',disk));

    end
```

```
%%%%%%%%%%%%%%%%%%%%%%%%%%%%%%%%%%
%% Establish points for diameter measurement
%%%%%%%%%%%%%%%%%%%%%%%%%%%%%%%%%%


    [L,n]=bwlabel(newBW,4);

    ded=regionprops(L,'Extrema');
    right_x= (ded.Extrema(3,1)+ded.Extrema(4,1))/2;
    right_y= (ded.Extrema(3,2)+ded.Extrema(4,2))/2;
    left_x= (ded.Extrema(7,1)+ded.Extrema(8,1))/2;
    left_y= (ded.Extrema(7,2)+ded.Extrema(8,2))/2;

    top_x= (ded.Extrema(1,1)+ded.Extrema(2,1))/2;
    top_y= (ded.Extrema(1,2)+ded.Extrema(2,2))/2;
    bottom_x= (ded.Extrema(5,1)+ded.Extrema(6,1))/2;
    bottom_y= (ded.Extrema(5,2)+ded.Extrema(6,2))/2;

%%%%%%%%%%%%%%%%%%%%%%%%%%%%%%%%%%
%% Image display while processing
%%%%%%%%%%%%%%%%%%%%%%%%%%%%%%%%%%
    %%Display the first 10 images and every 30th images; displays
    %%points used to measure diameter

    R=rem(i,30);                %function calculates remainder of i/30

    if i<10 || R==0
        imshow(newBW);
        hold on;

        plot(right_x,right_y,'ro');
        plot(left_x,left_y,'ro');
        plot(top_x,top_y,'bo');
        plot(bottom_x,bottom_y,'bo');
        m=i+offset;
        title_str=strcat('\fontsize {14} slide# = ', num2str(m));
        title(title_str);
        hold off;
        figure;
    end
%%%%%%%%%%%%%%%%%%%%%%%%%%%%%%%%%%
%% Establish initial radius in pixels for radial strain- can also set
manuallyImage display while processing
%%%%%%%%%%%%%%%%%%%%%%%%%%%%%%%%%%

    if i==1
        r_0_eq= ((left_y-right_y)^2+(left_x-right_x)^2)^.5;
                        %equitorial r_0 in pixels
        %r_0_eq=517     %for setting initial radius manually- in pixels
        r_0_sag= ((top_y-bottom_y)^2+(top_x-bottom_x)^2)^.5;
                        %sagittal r_0 in pixels

    end

    Radius_eq(i) = ((left_y-right_y)^2+(left_x-right_x)^2)^.5/r_0_eq;
                        % normalized equitorial radii
```

```
    Radius_sag(i) = ((top_y-bottom_y)^2+(top_x-bottom_x)^2)^.5/r_0_sag;
                            % normalized sagittal radii



    t(i)=i-1;
         % pictures taken every minute with time=0 for first image: i=1
    max_length=i;
    i=i+1;
end

%%%%%%%%%%%%%%%%%%%%%%%%%%%%%%%%%%
%% Plots of radial stain vs time and data output
%%%%%%%%%%%%%%%%%%%%%%%%%%%%%%%%%%

figure;
plot(t,Radius_eq,'r-');           %equitorial radius
hold on
plot(t,Radius_sag,'b-');          %sagital radius
for k=1:length(t)
    tt(k)=t(length(t)-k+1);
    rr(k)=Radius_eq(length(t)-k+1);
    rr_2(k)=Radius_sag(length(t)-k+1);
end


mat2=[tt; rr; rr_2];
mat3=mat2';                       %inverts rows and columns
dlmwrite('output.TAP',mat3,'\t'); %open this file with text editor and
                            then copy and paste into xcel
u=Radius_eq;

end
```

A. II. swelling_final_plot_TAP

```
function none=swelling_final_plot_TAP(ig)

%%To call function from command window:
%%swelling_final_plot_TAP([initial radius in microns, k_mushy guess,
%%bath concentration, zc])
%%example: final_plot_z_K_TEST([930,2e-15,.3,15])
%%Functions/files called:
%%swelling_calc_error_TAP.m
%%swelling_three_parameter_TAP.m
%%initiate_parameters_mouse_TAP.m
%%data_TAP.txt

tic
%%%%%%%%%%%%%%%%%%%%%%%%%%%%%%%%
%% Variables to set for each data set
%%%%%%%%%%%%%%%%%%%%%%%%%%%%%%%%

export_name ='malp_2_19_09_c_1';
date_name='2/19/09';

%%%%%%%%%%%%%%%%%%%%%%%%%%%%%%%%
%% Variables needed for plotting
%%%%%%%%%%%%%%%%%%%%%%%%%%%%%%%%
global tt;       % [-] normalized time
global rr;       % [-] normalized experimental radii
global r_theory; % [-] normalized radii from best fit line
global r0;       % [m] initial radius
global th;       % [hr] time in hours
global cout_percentage;  % concentration of bath solution[percentage
                  weight of solvent/ volume solute]
global z;        % [mol / m^3] fixed charge density
global h;        % [m] thickness of lens capsule
global er;       % [-] sum of squared error
global E;        % [Pa] Elasticity of lens capsule
global t_final;  % [min] final time
global K_mushy;  % [m^2/Pa/s] conductivity of the mushy zone

%%%%%%%%%%%%%%%%%%%%%%%%%%%%%%%%
%% Finding values of K_mushy and E to minimize sum of squared error
%%%%%%%%%%%%%%%%%%%%%%%%%%%%%%%%

r0 =  ig ( 1, 1 )*1e-6;      %initial radius given by the user
cout_percentage=ig ( 1, 3 ); %bath concentration given by user
z=ig ( 1, 4 );               %fixed charge density given by user

E_guess = initiate_parameters_mouse_TAP3;
                  %E initial guess is calculated from steady state
                  value
%E_guess=1e6;     %Set manually

initial_guess (1 , 1 )  = log ( E_guess );
initial_guess ( 2, 1 )  = log (ig ( 1, 2) );
                  % K_mushy initial guess given by the user
```

```
[X,FVAL,EXITFLAG,OUTPUT]=fminsearch('swelling_calc_error_TAP',
initial_guess ,optimset('tolX',1e-6))

%%%%%%%%%%%%%%%%%%%%%%%%%%%%%%%%%
%% Output
%%%%%%%%%%%%%%%%%%%%%%%%%%%%%%%%%

h_=h*1e6;          % thickness of lens capsule in microns

title_str=strcat('\fontsize {11} T_m_a_x= ', num2str(t_final),' min ,
C_o_u_t = ', num2str(cout_percentage) ,' % Saline, h=',num2str(h_),'um
, \fontsize {11} Error = ',num2str(er), ', \fontsize {12} E =
',num2str(E/1e6),' MPa');
x_info=strcat( ' K_M_u_s_h_y =',num2str(K_mushy), ' m^2/Pa/s  Zc=',
num2str(z),'  mil mol/lit');


output_matrix=[tt rr r_theory];
export_name2= strcat(export_name, '.tap');
wk1write('output',output_matrix);
dlmwrite(export_name2 ,output_matrix,'\t');



figure             % Plot radial strain vs normailzed time
plot (tt,rr,'.');
hold on;
plot (tt,r_theory,'r-');
X_LABEL_1=strcat(' \fontsize {15} t/t_f_i_n_a_l  \fontsize {12}
Date: ',date_name);
X_LABEL= strcat(X_LABEL_1, x_info);
xlabel(X_LABEL);
ylabel(' \fontsize {15} r/ro');
title(title_str);
%export_name
%print  ('-dtiff' ,export_name);
hold off



figure             %Plot time in hours
plot (th, rr, 'o','MarkerFaceColor','r','MarkerEdgeColor','r',
'MarkerSize',5 );
                   %plots time in hours
hold on;
plot (th,r_theory,'r-'); %plots time in hours
xlabel(' \fontsize {15} Time [hour]')
ylabel(' \fontsize {15} r/ro');
title(title_str);
hold off

toc
```

A. III. swelling_calc_error_TAP

```
function er = swelling_calc_error (k)

%%The return variable is the sum of squared error, which is minimized
%%in swelling_final_plot_TAP by iterating through values of E and K
%%mushy – starts with an initial guess for E at steady state and an
%%initial guess for K mushy given by the user
%%Function calls swelling_three_parameter_TAP
%%Function called by swelling_final_plot_TAP


%%%%%%%%%%%%%%%%%%%%%%%%%%%%%%%
%% Variables needed by swelling_final_plot_TAP
%%%%%%%%%%%%%%%%%%%%%%%%%%%%%%%

global tt;       % [-] normalized time
global rr;       % [-] normalized experimental radii
global r_theory; % [-] normalized radii from best fit line
global th;       % [hr] time in hours
global er;       % [-] sum of squared error
global E;        % [Pa] Elasticity of lens capsule
global t_final;  % [min] final time
global K_mushy;  % [m^2/Pa/s] conductivity of the mushy zone


%%%%%%%%%%%%%%%%%%%%%%%%%%%%%%%

E = exp (k(1));          %the log of E and K_mushy are being passed to
                         this function
K_mushy = exp (k(2));


%%%%%%%%%%%%%%%%%%%%%%%%%%%%%%%
%% Data import and resorting
%%%%%%%%%%%%%%%%%%%%%%%%%%%%%%%
file_name='data_TAP.txt';           % experimental results
mat = load (file_name);

raw_t = (mat(:,1));
raw_r = (mat(:,2));

t_final = raw_t(1);
x_final = raw_r(1);
max_l = length(raw_t);        %number of data points
rr=zeros(max_l,1);      %vector of length max_l - initialized to zeros
tt=zeros(max_l,1);

for i= 1:max_l
    tt(i)=raw_t(max_l-i+1)/t_final; %normalizing time
    th(i)=raw_t(max_l-i+1)/60;      %time in hours for plotting
    rr(i)=raw_r(max_l-i+1);         %radial strain
end

%%%%%%%%%%%%%%%%%%%%%%%%%%%%%%%
```

```
%%%%%%%%%%%%%%%%%%%%%%%%%%%%%%%%
%% Generation of additional values of time for the theoretical
calculations
%%%%%%%%%%%%%%%%%%%%%%%%%%%%%%%%
tt2=zeros(2*max_l-1,1);
j=1;
for i= 1:max_l

    tt2(j)=tt(i);
    j=j+1;
    if i<max_l
        tt2(j)=tt(i)+0.5/t_final;
        j=j+1;
    end
end

%%%%%%%%%%%%%%%%%%%%%%%%%%%%%%%%
%% Solving differential equation and calculating sum of squared error
%%%%%%%%%%%%%%%%%%%%%%%%%%%%%%%%
options=odeset('RelTol',1e-6,'AbsTol',1e-9);

[t,r_theor] = ode23s('swelling_three_parameter_TAP',tt2, 1, options);
%solves differential equation- tt is the timespan, 1 is the initial
radius r0

r_theory=zeros(max_l,1);
k=1;
for j= 1:2*max_l-1
    if tt(k)== t(j)
            r_theory(k)=r_theor(j);
            k=k+1;
    end
end


er = 0;
for i = 1:max_l
    er = er + ((r_theory(i) - rr(i))/rr(i))^2;
end

er = sqrt(er/ max_l);                %normalized sum of squared error
```

A. IV. swelling_three_parameter_TAP

```
function drdt = swelling_three_parameter_TAP(t,r_norm)

%%Function solves the differential equation drdt, and returns values
%%for the theoretical radial strain in time.
%%Function called by swelling_calc_error_TAP

%%%%%%%%%%%%%%%%%%%%%%%%%%%%%%%%%%
%% Parameters
%%%%%%%%%%%%%%%%%%%%%%%%%%%%%%%%%%
global E;         % [Pa] Elasticity of lens capsule
global K_mushy;   % [m^2/Pa/s] conductivity of the mushy zone
global lp;        % [m/Pa/s] hydraulic conductivity of lens capsule
global R;         % [m^3 Pa /K / mol] universal gas constant
global T;         % [K] temperature of bath
global h;         % [m] thickness of lens capsule
global nu;        % [-] Poisson ratio of lens capsule
global r0;        % [m] initial radius
global z;         % [mol / m^3] fixed charge density
global m;         % [mol / m^3] concentration of bath solution in metric
                    units
global t_fin;     % [s] final time in seconds


%%%%%%%%%%%%%%%%%%%%%%%%%%%%%%%%%%
%% Governing Equation Solution
%%%%%%%%%%%%%%%%%%%%%%%%%%%%%%%%%%
%See paper for derivation of governing equation

r=r_norm*r0;      %radius in microns

F_E_x_zc = (2/z)*sqrt(((E*h/(r0*(1-nu)*R*T))*(1-r0/r)+m)^2-m^2);
                  % F(E,x,zc)

rc = ((r0^3-F_E_x_zc*r^3)/(1-F_E_x_zc))^(1/3); %radius of core

firstterm = t_fin/r0; %to normalize- since experimental data is
                  % normalized

secondterm = 1/(1/lp+ (r-rc)/K_mushy);

thirdterm = 2*R*T* (sqrt(m^2 + (1/4)*z^2)-m );

forthterm = (2*E*h/(r0*(1-nu)))*(1-r/r0);

test= r0^3-F_E_x_zc*r^3; %when test goes negative, drdt has imaginary
                  %components from rc. It is set to zero at this point.

if test < 0
    drdt=0;
else
drdt= ( (firstterm*secondterm*(thirdterm - forthterm) ) );
end
```

A. V. error_contour_TAP

```
function error_contour_TAP(ig)

%%To call function from command window: error_contour_TAP([k_mushy from
%swelling_final_plot_TAP at e15,E from swelling_final_plot_TAP in MPa])
%%example: error_contour_TAP([2.2,1.7])
%%Function calculates the values of error along a K_mushy vs E grid to
%%ensure that the global minimum values are being obtained. Several
%%plots are generated (see "3D error grid and error plots" at end of
%%code). A spreadsheet is generated of values from which the 95%
%%confidence contour is calculated.
%%Functions/files called:
%%swelling_calc_error_TAP.m
%%swelling_three_parameter_TAP.m
%%initiate_parameters_mouse_TAP.m
%%data_TAP.txt

%%%%%%%%%%%%%%%%%%%%%%%%%%%%%%%%
%% Variables to set for each data set
%%%%%%%%%%%%%%%%%%%%%%%%%%%%%%%%

export_name ='malp_2_19_09_c_1_contour';
date_name='2/19/09';

%%%%%%%%%%%%%%%%%%%%%%%%%%%%%%%%
Ei = ig  ( 1, 2 )*1e6;
Kmj = ig ( 1, 1 )*1e-15;
initiate_parameters_mouse_TAP;      %need to make parameters global for
      %swelling_calc_error_TAP which calls swelling_three_parameter_TAP
global t_final;                     % [min] final time
global cout_percentage;             % concentration of bath
                    solution[percentage weight of solvent/ volume solute]
global z;                           % [mol / m^3] fixed charge density


tic
%%%%%%%%%%%%%%%%%%%%%%%%%%%%%%%%
%% Obtaining error values for K_mushy vs E grid
%%%%%%%%%%%%%%%%%%%%%%%%%%%%%%%%
for ii = -20:20                 %percent scanning over E
min_error=1;
    for jj = -20:20                     %percent scanning over K mushy
       i= ii+21;
       j= jj+21;                        %when plotting, the array values
                                        cannot be negative

        E_guess = Ei + Ei*ii/100 ;
        K_m_guess = Kmj + Kmj*jj/100;

        initial_guess (1 , 1 )  = log ( E_guess );
                                % E initial guess is calculated from the
                                steady state value

        initial_guess ( 2, 1 )  = log (K_m_guess );
                                % K_mushy initial guess given by the user
```

```
        format short eng

        error_test =  swelling_calc_error_TAP (initial_guess);

        format short

        x_out (i) =  E_guess*1e-6;                  %MPa
        y_out (j) = K_m_guess*1e16;
        error_out (j,i) = error_test;

        if(error_test < min_error)
                              %finding values of min error at each
                            value of E
            min_error=error_test;
            E_error= E_guess;
            K_error= K_m_guess;
        end
    end

      min_out_error (i) = min_error;
                          %for each value of E, saving the min error and
                          %K mushy at the min error; used for plotting
      min_out_E (i) = E_error;
      min_out_K (i) = K_error;

end

toc

%%%%%%%%%%%%%%%%%%%%%%%%%
%% Output
%%%%%%%%%%%%%%%%%%%%%%%%%

mat2=[error_out];  %Matrix of the error for each combination of K and E

export_name2= strcat(export_name, '.tap');
dlmwrite(export_name2 ,mat2,'\t');

%Open with text editor - Select All (Cntl A) - Paste into Microsoft
Xcel. This gives a grid of the error for each combination of K and E.
Can calculate the error confidence intervals from this. E changes along
the rows; K changes along the columns.


%%%%%%%%%%%%%%%%%%%%%%%%%
%% 3D error grid and error plots
%%%%%%%%%%%%%%%%%%%%%%%%%

TITLE=strcat('\fontsize {11}Date:',date_name, ' T_m_a_x= ',
num2str(t_final),' min , C_o_u_t = ', num2str(cout_percentage) ,' %
Saline, Zc=', num2str(z),'  mil mol/lit');

figure                %Contour of error at each combination of K and E
surfc(x_out,y_out,error_out);
shading faceted;
```

```
colorbar
view(0,0)
xlabel('\fontsize {30} E [MPa]');
ylabel('\fontsize {30} K_m [m^2/Pa/s]');
%print  ('-dpdf' ,export_name2);


figure                  %Contour of error at each combination of K and E
                            at a different view
surfc(x_out,y_out,error_out)
xlabel('\fontsize {30} E [MPa]');
ylabel('\fontsize {30} K_m [m^2/Pa/s]');
zlabel('\fontsize {30} error')
title(TITLE)
colorbar
%print  ('-dpdf' ,export_name2);


figure                          %Plot of minimum value of error at each E
plot(min_out_E, min_out_error, 'md')
title(TITLE)
xlabel('\fontsize {30} E [MPa]')
ylabel('\fontsize {30} error')

figure                         %Plot of the K that gives the minimum
                                value of error in E at each E
plot(min_out_E, min_out_K, 'md')
title(TITLE)
xlabel('\fontsize {30} E [MPa]')
ylabel('\fontsize {30} K_m [m^2/Pa/s]')
```

A. VI. data_TAP.txt

Data file that contains the output from get_time_radius_TAP. Consists of two columns: column one is time in minutes in descending order; column two is the radial strain at each point in time.

APPENDIX B: Computational Model

B I. Nomenclature

A = spherical surface area of lens capsule [m^2]

E = modulus of elasticity of lens capsule [Pa]

J_v = solvent volumetric flux into lens fiber cells [$m \cdot s^{-1}$]

K_m = Darcy conductivity of the mushy zone [$m^2 \cdot Pa^{-1} \cdot s^{-1}$]

K_T = total hydraulic conductivity of lens capsule-mushy zone system [$m \cdot Pa^{-1} \cdot s^{-1}$]

L_p = hydraulic conductivity of the lens capsule [$m \cdot Pa^{-1} \cdot s^{-1}$]

P = hydrostatic pressure [Pa]

R = universal gas constant [= 8.314 m^3 $Pa \cdot K^{-1} \cdot mol^{-1}$]

T = ambient temperature [= 293 K]

V = volume of spherical lens [m^3]

$[X^+]$ = concentration of positive monovalent ions [$mol \cdot m^{-3}$]

$[Y^-]$ = concentration of negative monovalent ions [$mol \cdot m^{-3}$]

h = thickness of lens capsule [m]

m = concentration of solute outside the lens [$mol \cdot m^{-3}$]

r = lens equatorial radius [m]

r_c = core equatorial radius [m]

r_0 = initial lens equatorial radius [m]

t = time [s]

zc = fixed charge density of core [$mol \cdot m^{-3}$]

v = Poisson's ratio of lens capsule [-]

π = osmotic pressure [Pa]

B II. Water Flux from Bath into Lens

The osmotic pressure difference between the core and the bath is the driving force for water movement through the lens capsule and the mushy zone. The lens increases in volume from the water influx until the osmotic pressure is balanced by the mechanical pressure exerted by the lens capsule. The solvent flux J_v is related to the spherical lens expansion:

$$J_v = \frac{1}{A}\frac{dV}{dt} = \frac{dr}{dt} \tag{B1}$$

where V and A are the total volume and the surface area of the spherical lens, respectively. The flux across the lens capsule and the mushy zone is specified by the Kedem–Katchalsky equation [45]:

$$J_v = K_T(\Delta\pi_{c-o} - \Delta P_{c-o}) \tag{B2}$$

where K_T is the total hydraulic conductivity of the system (mushy zone and capsule) and $\Delta\pi_{c\text{-}o}$ and $\Delta P_{c\text{-}o}$ are the osmotic and hydrostatic pressure differences between the outside bath and the core, respectively.

B III. Hydraulic Conductivity

Water must cross both the lens capsule and the mushy zone to reach the core. As the mushy zone increases in thickness, further swelling occurs more slowly due to the increased travel distance required for water to reach the core. Water moves through the lens capsule and the mushy zone in series, which results in the following expression for total hydraulic conductivity:

$$K_T = \left(\frac{1}{L_p} + \frac{r - r_c}{K_m} \right)^{-1} \tag{B3}$$

The hydraulic conductivity of the lens capsule, L_p, is reported as velocity per unit pressure difference. The Darcy hydraulic conductivity of the mushy zone, K_m is in velocity per unit pressure gradient and is one of the two parameters regressed by the experimental data. The parameters r and r_c are the radius of the lens and the radius of the core as functions of time.

B IV. Hydrostatic Pressure Difference between Core and Bath

For a spherical isotropic, linear elastic shell with thickness h << radius r, the pressure difference across the shell is given by [44]:

$$\Delta P_{c-o} = \frac{2Eh\varepsilon}{r(1-\nu)} \tag{B4}$$

where E is the modulus of elasticity of the lens capsule, the second parameter regressed by the experimental data; h is the thickness of the lens capsule, obtained from literature [51]; r is the radius of the lens in time, obtained from experimental data; and ν is Poisson's ratio of the lens capsule, obtained from literature [25,61]. The circumferential strain ε can be written in terms of r and the initial radius r_0, obtained from experimental data:

$$\varepsilon = \frac{2\pi r - 2\pi r_0}{2\pi r_0} = \left(\frac{r}{r_0} - 1 \right) \tag{B5}$$

This gives:

$$\Delta P_{c-o} = \frac{2Eh}{r_0(1-\nu)}\left(1-\frac{r_0}{r}\right) \tag{B6}$$

B V. Osmotic Pressure Difference between Core and Bath

The osmotic pressure difference between the core and the outside bath is modeled based on the assumption of a uniform, monovalent charge distribution within the core. As previously stated, two types of ions are present in the system: one group is the fixed charges with a charge density of *zc*, and the second group is the free ions. Free ions are lumped into a representative positive ion [X^+] and a representative negative ion [Y^-], both monovalent (Fig. 3C, p 8). The subscripts *c* and *o* refer to the core of the lens and the outside bath, respectively. Compared to the solvent, the free charges are assumed to transport quickly enough that the Donnan equilibrium [47] is achieved instantaneously:

$$\left[X^+\right]_c\left[Y^-\right]_c = \left[X^+\right]_o\left[Y^-\right]_o \tag{B7}$$

Since the lens volume is approximately 100-fold smaller than the bath volume, the bath concentration of ions, *m*, is taken to remain unchanged during the course of experiment:

$$\left[X^+\right]_o = \left[Y^-\right]_o = m \tag{B8}$$

From Eq. (B7) and (B8):

$$\left[X^+\right]_c\left[Y^-\right]_c = m^2 \tag{B9}$$

Considering the fixed charges to be negative [46,62], electroneutrality inside the lens requires that the free charges equilibrate with the fixed charges in the lens fiber cells [47]:

$$\left[X^+\right]_c = \left[Y^-\right]_c + zc \tag{B10}$$

Substituting Eq. (B10) into Eq. (B9):

$$\left(\left[Y^-\right]_c + zc\right)\left[Y^-\right]_c = m^2 \tag{B11}$$

$$\left[Y^-\right]_c^2 + (zc)\left[Y^-\right]_c - m^2 = 0 \tag{B12}$$

$$\left[Y^-\right]_c = \frac{-(zc) \pm \sqrt{(zc)^2 + 4m^2}}{2} \tag{B13}$$

Concentration must be a positive real number, so the valid solution is:

$$\left[Y^-\right]_c = \frac{-(zc) + \sqrt{(zc)^2 + 4m^2}}{2} \tag{B14}$$

From Eq. (B10) and (B14):

$$\left[X^+\right]_c = zc + \frac{-(zc) + \sqrt{(zc)^2 + 4m^2}}{2} = \frac{zc + \sqrt{(zc)^2 + 4m^2}}{2} \tag{B15}$$

The concentration of the free charges in the core is the sum of the positive and negative free charges:

$$C_c = \left[X^+\right]_c + \left[Y^-\right]_c = 2\frac{\sqrt{(zc)^2 + 4m^2}}{2} = 2\sqrt{\frac{(zc)^2}{4} + m^2} \tag{B16}$$

Similarly, the concentration of the free charges in the hypotonic bath solution, with Eq. (B8), gives:

$$C_o = \left[X^+\right]_o + \left[Y^-\right]_o = 2m \tag{B17}$$

The difference in concentration between the core and the bath solution is:

$$\Delta C_{c-o} = C_c - C_o \tag{B18}$$

$$\Delta C_{c-o} = 2\sqrt{\frac{(zc)^2}{4} + m^2} - 2m \tag{B19}$$

From Eq. (B19) and the Van't Hoff relation [63]:

$$\Delta\pi = RT\Delta C \tag{B20}$$

where ΔC is the difference in solute concentration, the osmotic pressure difference between the core and outside bath is:

$$\Delta\pi_{c-o} = 2RT\left(\sqrt{m^2 + \frac{(zc)^2}{4}} - m\right) \tag{B21}$$

where R is the universal gas constant, T (=293 K) is the ambient temperature, and *zc* is the fixed charge density.

B VI. Radius of Core with Time

The change in core radius with time is needed for the computation of the total hydraulic conductivity. The osmolarity of the mushy zone never reaches that of the outside bath concentration due to the resistance to expansion of the lens capsule. The equilibrium of the hydrostatic and osmotic pressures between the mushy zone and the hypotonic solution gives:

$$\Delta\pi_{m-o} = \Delta P_{m-o} \tag{B22}$$

A pressure gradient cannot be supported within the lens, resulting in an equilibrated hydrostatic pressure between the mushy zone and core:

$$P_{mushy} = P_{core} \tag{B23}$$

Equation (B23) can be incorporated into Eq. (B6) to give the pressure difference between the bath and the mushy zone. As water moves into the mushy zone, the fractional volume of water increases and, resultantly, the fixed charge density decreases. The change in fixed charge density must be factored into Eq. (B21) to calculate the osmotic pressure difference between the mushy zone and the outside bath. A term involving a volumetric ratio accounts for the change in concentration. Choosing a specific point in time and assigning the total number of fixed charges within the mushy zone to *N(t)*:

$$zc_m(t) = \frac{N(t)}{V_m(t)} \tag{B24}$$

Considering the lens fibers within the mushy zone at this point in time, before swelling began, the same fibers had a charge density of:

$$zc = \frac{N(t)}{V_{m0}(t)} \tag{B25}$$

The number of charges has not changed within the specific zone because the number of lens fiber cells has not changed. Combining Eq. (B24) and (B25) gives:

$$\frac{zc_m(t)}{zc} = \frac{V_{m0}(t)}{V_m(t)} \tag{B26}$$

$$zc_m(t) = zc\frac{V_{m0}(t)}{V_m(t)} \tag{B27}$$

From section B V., the concentration of ions within the core is:

$$C_c = \left[X^+\right]_c + \left[Y^-\right]_c = 2\frac{\sqrt{(zc)^2 + 4m^2}}{2} = 2\sqrt{\frac{(zc)^2}{4} + m^2} \tag{B16}$$

The fixed charge density *zc* in the core is the concentration before swelling, which is the *in vivo* concentration. The concentration of ions within the mushy zone is give by the following equation, where $zc_m(t)$ is used in place of *zc*:

$$C_m = 2\sqrt{\frac{(zc_m(t))^2}{4} + m^2} \tag{B28}$$

Incorporating Eq. (B27) into Eq. (B28) gives:

$$C_m = 2\sqrt{\left(\frac{V_{m0}}{V_m}\right)^2\frac{(zc)^2}{4} + m^2} \tag{B29}$$

In combination with Eq. (B17) and (B18):

$$\Delta C_{m-o} = 2\sqrt{\left(\frac{V_{m0}}{V_m}\right)^2 \frac{(zc)^2}{4} + m^2} - 2m \tag{B30}$$

From the Van't Hoff relation, Eq. (B20), the osmotic pressure between the mushy zone and the bath is:

$$\Delta\pi_{m-o} = 2RT\left(\sqrt{m^2 + \left(\frac{V_{m0}}{V_m}\right)^6 \frac{(zc)^2}{4}} - m\right) \tag{B31}$$

Using the assumption that the lens is spherical, the geometry of the system gives:

$$V_c = V - V_m = V_0 - V_{m0} \tag{B32}$$

$$V_{m0} = V_0 - V_c \tag{B33}$$

$$V_m = V - V_c \tag{B34}$$

$$\frac{V_{m0}}{V_m} = \frac{V_0 - V_c}{V - V_c} \tag{B35}$$

$$\frac{V_{m0}}{V_m} = \frac{r_0^{\,3} - r_c^{\,3}}{r^3 - r_c^{\,3}} \tag{B36}$$

Combining Eq. (B31) and (B36):

$$\Delta\pi_{m-o} = 2RT\left(\sqrt{m^2 + \left(\frac{r_0^{\,3} - r_c^{\,3}}{r^3 - r_c^{\,3}}\right)^2 \frac{(zc)^2}{4}} - m\right) \tag{B37}$$

Combining Eq. (B6), (B22), (B23), and (B37) gives:

$$2RT\left(\sqrt{m^2+\left(\frac{r_0^{\,3}-r_c^{\,3}}{r^3-r_c^{\,3}}\right)^2\frac{(zc)^2}{4}}-m\right)=\frac{2Eh}{r_0(1-\nu)}\left(1-\frac{r_0}{r}\right) \tag{B38}$$

Solving for the radius of the core, r_c gives:

$$r_c=\left(\frac{r_0^3-f(E,r,zc)r^3}{1-f(E,r,zc)}\right)^{1/3} \tag{B39}$$

where

$$f(E,r,zc)=\frac{2}{zc}\sqrt{\left[\frac{Eh}{r_0(1-\nu)RT}\left(1-\frac{r_0}{r}\right)+m\right]^2-m^2} \tag{B40}$$

B VII. Governing Equation

Combining Eq. (B1) through (B40) yields a single governing ODE:

$$\frac{dr}{dt}=\left(\frac{1}{L_p}+\frac{r-\sqrt[3]{\dfrac{r_0^3-f(E,r,zc)r^3}{1-f(E,r,zc)}}}{K_m}\right)^{-1}\left[2RT\left(\sqrt{m^2+\frac{(zc)^2}{4}}-m\right)-\frac{2Eh}{r_0(1-\nu)}\left(1-\frac{r_0}{r}\right)\right] \tag{B41}$$

APPENDIX C: **NaCl Bath Concentration Unit Conversion**

Osmotic swelling was achieved through placement of lenses in a hypotonic saline solution: 0.1%, 0.2%, or 0.5% w/v for porcine lenses and 0.3% or 0.5% for mouse lenses. The hypotonic solutions were made by dissolving the appropriate mass of NaCl into de-ionized water; for example, 1.00 g of NaCl was mixed into 1.00 L of DI water to obtain the 0.1% solution. For use in the computational model, the NaCl concentration must be converted from % weight/volume to mol• m^{-3}. A 1% w/v solution is equivalent to 0.01 kg/L or 10 g/L, and the molecular weight of Na and Cl are 22.989 and 35.453 g/mol, respectively. The following calculation demonstrates the conversion of 0.1 % w/v to mol• m^{-3}:

$$\frac{.1\%w/v\left(10\frac{g/L}{w/v}\right)\left(1000\frac{L}{m^3}\right)}{\left(22.989\frac{g}{mol}+35.453\frac{g}{mol}\right)}=17.11\frac{mol}{m^3} \tag{C1}$$

The conversions for all of the hypotonic solutions are listed in Table C1.

Table C1: NaCl Bath Concentration Unit Conversion

% w/v	mol• m^{-3}
0.1	17.11
0.2	34.22
0.3	51.33
0.5	85.56

APPENDIX D: Literature and Fitted Constants

D I. Modulus of Elasticity, *E*

Similar to most biological materials, the stress-strain curve for the lens capsule shows a high degree of nonlinearity [24]. In the low strain region (below 10%), the curve is nearly linear, giving a constant elastic modulus. Although most reported mechanical properties come from studies on the anterior portion of the lens capsule, in the low strain region, the elastic moduli of the anterior and posterior lens capsules are almost identical [23].

Most of the osmotic swelling occurs in the low strain region, where the lens capsule is linearly elastic. It is assumed that the lens capsule is uniformly, linearly elastic for the computational model. The modulus of elasticity is an optimization parameter in the MATLAB simulation model.

D II. Capsule Thickness, *h*

The thickness of the lens capsule varies with age and location [22,49,50], as mapped in detail by Barraquer et al. [50]. The thickest area of the lens is located at the mid-periphery of anterior and posterior lens.

Danysh et al. [49] measured the lens capsule thickness of young (7-9 weeks) and old (24 to 29 weeks) mice from four inbred strains and one out-bred strain. They found that thickness varied between inbred strains, suggesting that it is a quantitative genetic trait. The anterior capsule thickness was statistically similar in the young mice, with the

exception of the strain with a collagen IV defect, but varied significantly between strains as the mice aged.

The thicknesses of the anterior pole, equatorial position, and posterior pole were measured in one of the wild-type strains at 10 weeks: 11.4μm, 9.4μm, and 2.5μm, respectively. The ratio of 4.5 for the anterior to posterior region thickness of mouse lenses is consistent with the ratio for porcine lenses, which ranges from 3 to 5 [22].

For this study, the equatorial diameter from mice 8 weeks old is used in the computational model. A constant thickness of 9.4μm is used since the values measured by Danysh et al. were comparable in different strains of young mice. It is important to recognize that the areas above and below the equator are the thickest regions of the capsule and, therefore, the stiffest. These regions may restrict the equatorial region from reaching the strain it would if the entire capsule was of uniform thickness.

For the porcine lens, the average thickness of the anterior surface [51] is used for the average thickness of the entire lens capsule. Since the anterior capsule is thicker than the posterior capsule [22], the model computes a modulus of elasticity for a stiffer lens capsule than the physiological capsule.

D III. Darcy Hydraulic Conductivity of Mushy Zone, K_m

The Darcy hydraulic conductivity of mouse lens fiber cells has been measured [39,64]. However, the water permeability of lens fibers in a swollen state, as they are in the mushy zone, has not been measured. The Darcy Conductivity of the mushy zone is, therefore, an optimization parameter in the MATLAB simulation model.

D IV. Capsule Hydraulic Conductivity, L_p

A measurement of the hydraulic conductivity of the lens capsule was not found in literature for the mouse. The hydraulic conductivity of the rabbit, cow, pig, and rat lens capsules are on the same order of magnitude [4,65,66]. The hydraulic conductivity of rat lens capsules, 4.76 ± .73 x 10-11 m/s•Pa [4], is used in the computational model. The hydraulic conductivity of the mouse lens capsule will be determined in a later study for wild type and Alport mice.

D V. Fixed Charge Density of Lens Fiber Cells, *zc*

The fixed charges are associated with proteins and macromolecules within the lens fiber cells that cannot cross the cell membrane. They are assumed to be negative [62], and only one report of the fixed charge density in lens fiber cells was found in literature [46]. The fixed charge density is, therefore, treated as a fitting parameter in the MATLAB computational model within the range of Bartels and Elliott's findings [46].

D VI. Poisson's Ration, *v*

The Poisson's ratio for human and cat lens capsules was experimentally measured to be 0.47, with no observed change with age [25]. The Poisson's ratio for an age 11 human lens capsule was estimated to be 0.46 with computational modeling [61].

APPENDIX E: **Confidence Interval Calculations**

Draper and Smith [53] provide an expression for determining a 100*(1-α)% confidence region for *n* sets of observation in a *p*-dimensional parameter space (p. 497 and 504):

$$S(\theta) = S(\hat{\theta})\left\{1 + \frac{p}{n-p} F(p, n-p, 1-\alpha)\right\}$$

For most of the porcine data sets, a picture was taken every 5 or 10 minutes for 10 hours, giving an *n* of 121 and 61 respectively. Pictures of the mouse lenses were taken every minute for 3 hours, giving an *n* of 181. The modulus of elasticity *E* and Darcy conductivity of the mushy zone K_m are the two parameters, which generate a 2-dimensional parameter space: p is two.

Mouse (3 hours of data):

$$S(\theta) = S(\hat{\theta})\left\{1 + \frac{2}{181-2} F(2,179,.95)\right\} = S(\hat{\theta})\{1 + (0.01117)(3.046)\} = S(\hat{\theta})\{1.034\}$$

Porcine (pictures taken every 5 minutes)/ Mouse (2 hours of data):

$$S(\theta) = S(\hat{\theta})\left\{1 + \frac{2}{121-2} F(2,119,.95)\right\} = S(\hat{\theta})\{1 + (0.0168)(3.072)\} = S(\hat{\theta})\{1.052\}$$

Porcine (pictures taken every 10 minutes)/ Mouse (1 hour of data):

$$S(\theta) = S(\hat{\theta})\left\{1 + \frac{2}{61-2} F(2,59,.95)\right\} = S(\hat{\theta})\{1 + (0.0339)(3.153)\} = S(\hat{\theta})\{1.107\}$$